Analytic description of high-order harmonic generation in the adiabatic limit with application to an initial s state in an intense bicircular laser pulse

M. V. Frolov, N. L. Manakov, A. A. Minina, A. A. Silaev, N. V. Vvedenskii, M. Yu. Ivanov, and Anthony F. Starace

Phys. Rev. A **99**, 053403 — Published 2 May 2019

DOI: 10.1103/PhysRevA.99.053403

Analytic description of high-order harmonic generation in the adiabatic limit with application to an initial s-state in an intense bicircular laser pulse

M.V. Frolov,[1] N.L. Manakov,[1] A.A. Minina,[1] A.A. Silaev,[1,2,3]
N.V. Vvedenskii,[1,2,3] M.Yu. Ivanov,[4,5,6] and Anthony F. Starace[7]

[1] *Department of Physics, Voronezh State University, Voronezh 394018, Russia*
[2] *Institute of Applied Physics, Russian Academy of Sciences, Nizhny Novgorod 603950, Russia*
[3] *University of Nizhny Novgorod, Nizhny Novgorod 603950, Russia*
[4] *Max-Born Institute, Max-Born-Strasse 2A, Berlin D-12489, Germany*
[5] *Blackett Laboratory, Imperial College London, South Kensington Campus, SW7 2AZ London, United Kingdom*
[6] *Department of Physics, Humboldt University, Newtonstrasse 15, 12489 Berlin, Germany*
[7] *Department of Physics and Astronomy, The University of Nebraska, Lincoln NE 68588-0299, USA*

(Dated: April 8, 2019)

An analytic description of high-order harmonic generation (HHG) is proposed in the adiabatic (low-frequency) limit for an initial s-state and a laser field having an arbitrary waveform. The approach is based on the two-state time-dependent effective range theory and is extended to the case of neutral atoms and positively-charged ions by introducing *ad hoc* the Coulomb corrections for HHG. The resulting closed analytical form for the HHG amplitude is discussed in terms of *real* classical trajectories. The accuracy of the results of our analytic model is demonstrated by comparison with numerical solutions of the time-dependent Schrödinger equation for a strong bicircular field comprised of two equally intense components with carrier frequencies ω and 2ω and opposite helicities. In particular, we demonstrate the effect of ionization gating on HHG in a bicircular field, both for the case that the two field components are quasimonochromatic and for the case that the field components are time-delayed short pulses. We show how ionization in a strong laser field not only smooths the usual peak structures in HHG spectra, but also changes the positions and polarization properties of the generated harmonics, seemingly violating the standard dipole selection rules. These effects appear for both short and long incident laser pulses. In the case of time-delayed short laser pulses, ionization gating provides an effective tool for control of both the HHG yield and the harmonic polarizations [M.V. Frolov *et al.*, Phys. Rev. Lett. **120**, 263203 (2018)]. For the case of short laser pulses, we introduce a simple two-dipole model that captures the physics underlying the harmonic emission process, describing both the oscillation patterns in HHG spectra and also the dependence of the harmonic polarizations on the harmonic energy.

I. INTRODUCTION

High-order harmonic generation (HHG) is an effective tool for converting intense low-frequency laser radiation into coherent high-frequency radiation. This nonlinear light conversion process has found a wide range of practical applications in laser physics [1], including in development of table-top sources of coherent X-ray light [2–4], in attosecond pulse generation and attosecond spectroscopy [5, 6], and in ultrafast spectroscopy in general (see, e.g., Refs. [7, 8]). The importance of HHG has consequently stimulated many experimental and theoretical studies aimed at understanding this nonlinear process.

The theoretical description of HHG and other nonlinear processes in a strong nonperturbative laser field encounters several obstacles, which remain a challenge even a half-century after the advent of strong field physics [9, 10]. The key challenge is the need to describe the nonperturbative laser field on the same footing as the field of the ionic core, as together they govern the electron dynamics. While this challenge is met by numerical solutions of the time-dependent three-dimensional Schrödinger equation (TDSE), exact solutions are only rarely possible. Even in the single-active-electron approximation (see, e.g., Refs. [8, 11–13]), numerical simulations are feasible only in limited ranges of the laser parameters. For example, numerical simulations of the nonlinear interactions in the very important regime of intense mid-infrared (MIR) fields, e.g., for wavelengths $\gtrsim 3\mu$m, are numerically extremely challenging, especially in the case when the polarization of laser pulse is not linear. Simulations for elliptically polarized laser pulses or for those having unusual spatial waveforms are rather difficult and require special treatments [14–17]. Including multielectron correlations is more difficult still, with practical algorithms limited to the case of linear polarization and restricted frequency and intensity ranges [18–26].

Although exact numerical solution of the TDSE remains the premier theoretical method, owing to its limited range of applicability, the development of quantitative analytical theories, benchmarked against accurate numerical simulations, have a role to play in the analysis of HHG. This is especially true in parameter regions currently inaccessible to accurate numerical analysis, such as, e.g., in the MIR frequency range. In such cases, analytical methods and models can enable significant advances in physical understanding.

The workhorse of strong field physics is the strong field approximation (SFA) [27, 28], whose essential ideas were formulated in the 1960s and 1970s [29–33]. The main idea is to consider the interaction of the laser field with an active atomic electron exactly, while either neglecting the electron-atom interaction following ionization (in zero order) or taking it into account perturbatively. This approach leads to a formal Born-like series (in the atomic potential) for transition amplitudes, the convergence of which remains an open mathematical question. In practice, however, the first few terms of such an expansion (as in the so-called "improved" SFA) are sufficient to describe the general features of HHG [27, 34–38].

Crucially, the SFA led to a very important insight into the theoretical description of strong field phenomena, namely, the applicability of the quantum orbit approach (QOA) [34, 39–42]. In terms of the QOA, the HHG amplitude is represented as a sum of partial amplitudes, each of which is associated with a complex closed electron trajectory in the laser field. These trajectories formally satisfy Newton's equations, although they correspond to complex starting and ending times that are found from adiabaticity conditions [43] for the ionization and recombination steps [34, 39–42]. In the strong field limit, the QOA results are in good agreement with SFA results. Moreover, the QOA provides a natural means of including the Coulomb-induced corrections to the HHG amplitude within quasiclassical perturbation theory [44]. (In the quasiclassical limit, the HHG process may be split into its well-known three steps [45]: ionization, propagation, and recombination.) A similar picture of quantum orbits also naturally arises within the analytical R-matrix theory [46–50], which uses semiclassical perturbation theory in the action to include the effects of the Coulomb potential on strong-field-driven electron dynamics. Using the QOA and either quasiclassical perturbation theory or the analytical R-matrix theory, Coulomb corrections may be derived for the first two steps of the HHG process [50–52], including Coulomb corrections to the ionization and recombination times.

The quantum orbits picture thus provides a natural basis for alleviating the main drawback of the SFA, the lack of an accurate treatment of the electron-core interaction. It suggests introducing *ad hoc* corrections to the SFA amplitude, utilizing the known parametrization of the HHG amplitude [53, 54]. The key corrections amount to replacing the plane-wave photorecombination amplitude by the exact one [37, 38] and using accurate strong-field ionization amplitudes. This approach has now been successfully extended to HHG in molecules, including multi-electron effects during ionization, active electron motion in the continuum, and recombination (see, e.g., Refs. [42, 55–60]). Applications include analysis of enantio-sentitivity of HHG in chiral molecules [61–63], description of HHG by atoms with initial p-orbitals [64, 65], and control of the spin-polarization of recolliding electrons [66].

The study of strong field phenomena has also been greatly advanced by exactly-solvable analytical models. The first such model of an atomic system in a strong laser field was the δ-potential (or zero-range potential) model [67]. It was used initially to describe the detachment of a weakly-bound electron in a negative ion induced by a nonperturbative ac-field [68–70]. Later it was extended to describe the HHG process [71, 72]. A main drawback of the δ-potential model is that its practical application is restricted to systems with weakly-bound electrons in an initial s-state. Its extension to the case of higher angular momenta in the initial bound state was achieved within the time-dependent effective range (TDER) approach [73, 74]. This method combines the effective range theory for the description of the non-perturbative electron interaction with an atomic core [75, 76] and the Floquet-formalism-based quasistationary quasienergy description of the electron interaction with a nonperturbative laser field [68, 77]. It coincides with the δ-potential model in an appropriate limit.

In a periodic laser field, the HHG process can naturally be treated within the TDER model using the relation between the complex quasienergy and the HHG amplitude [78]. For short laser pulses, direct application of the Floquet formalism is impossible, but appropriate extensions of the TDER model have been developed [79, 80]. A one-dimensional δ-potential model has also been successfully used to analyze HHG for the case of a few-cycle laser pulse [81].

The main advantage of the analytical models is their innate applicability in the low-frequency regime of MIR laser fields, precisely where numerical simulations become prohibitively expensive. The analytical structure of the HHG amplitude in this regime has been studied in detail [54, 80–85]. For the case of linear polarization, these results provide a rigorous theoretical justification for the factorization of the HHG yield as the product of an electronic wave packet (EWP) and the exact photorecombination cross section [54, 80–84], as was suggested in Refs. [53, 86, 87] based upon numerical TDSE results. However, for both the case of an elliptically polarized monochromatic laser field [17, 84] and the case of a two-color laser field having orthogonal linearly polarized monochromatic components [85] other parametrizations of the HHG amplitude were obtained, different from that for the case of linear polarization.

In this paper we develop an analytic description of the HHG amplitude for the case of a laser field having an arbitrary spatial and temporal waveform. Although experimental data exist for some complex field configurations [88, 89], up to now there have been no corresponding analytical studies. More specifically, for an active electron in an initial s-state we develop here an analytical description of HHG applicable in the low-frequency (or adiabatic) limit for a laser pulse having an arbitrary spatial and temporal waveform. We then apply this theory to the case of HHG driven by a bicircular laser field comprised of pulses having carrier frequencies ω and 2ω and opposite circular polarizations. Both the low-frequency approximation and the case of HHG driven by a bicircular laser field have long histories, which we summarize briefly and relate to the present work prior to presenting the organization of this paper.

The low-frequency (or adiabatic) approximation for the case of ionization of a weakly bound electron in a zero-range potential driven by an elliptically polarized laser field was analyzed in 1980 using the quasistationary quasienergy state formalism [70]. More recently, an alternative adiabatic approximation formalism has been employed to analyze both ionization [90] and HHG [81] for the case of an electron bound in a zero-range potential and interacting with a linearly polarized laser field; its use for the case of ionization of an electron in a finite range potential has also been studied [91]. Most recently, the low-frequency approximation has been used to study HHG driven by bicircular (monochromatic) laser fields [38]. The physics of the low-frequency (or adiabatic) approximation is similar to that used by P.L. Kapitza to describe a particle in a rapidly oscillating field in classical mechanics [92, 93]. Specifically, the time-dependent (periodic in time) wave function is decoupled into slowly and rapidly changing parts, where the latter part is found using a basis unperturbed by the laser field, while the slowly changing part is found including effects of the rapidly changing part. Such decoupling can be realized in the case of a slowly changing laser field (relative to an atomic time scale) [91].

The study of HHG driven by a bicircular laser field was initiated over twenty years ago [94, 95]. It has become a very hot topic recently, both experimentally and theoretically, owing to the polarization properties of high harmonics generated in such fields. Specifically, the use of bicircular driving laser fields has been shown to produce circularly or elliptically polarized harmonics or attosecond pulses [38, 88, 94–103]. Moreover, means for controlling the polarization of the emitted coherent radiation have been proposed and/or experimentally demonstrated [64, 88, 89, 94, 95, 97, 99–110]. There exist many important applications of isolated short laser pulses in the extreme ultraviolet and X-ray regimes with controlled polarization for studying chiral-sensitive light-matter interactions in, e.g., magnetic materials [88, 97, 100, 111–113] or polyatomic molecules [58, 96, 101, 108, 114].

Note that existing theoretical descriptions of HHG in a bicircular field are based on the SFA [64, 65, 95, 98, 107, 115], which ignores effects of the Coulomb potential. In a recent study [38], the low-frequency approximation is employed to analyze the HHG amplitude and it is shown how the exact photorecombination amplitude (for the studied atomic model) appears in that amplitude. However, although Coulomb phases are introduced *ad hoc*, the analysis is mainly suitable for short-range potentials, as the boundary conditions for the wave function at large distances do not take into account the long-range Coulomb interaction. Thus, additional Coulomb corrections to the HHG amplitude (taking into account ionization and propagation in the Coulomb field) are required [51, 52].

This paper is organized as follows. In Sec. II we generalize our two-state TDER model for HHG, which initially was developed for a linearly polarized monochromatic field [54], to the general case of a driving laser pulse having an arbitrary spatial and temporal waveform. In Sec. III we discuss the extension of our theory to neutral atoms and positively-charged ions. A number of applications for the case of a bicircular driving field are presented in Sec. IV, including results for both long and short driving laser fields, a comparison with numerical solutions of the TDSE, a trajectory analysis, and, for the case of short bicircular fields, a two-dipole model for HHG emission. We summarize our results and present our conclusions in Sec. V. Some mathematical details and derivations concerning the HHG amplitude and the recombination dipole moment are presented in Appendices A, B, C, and D. Atomic units (a.u.) are used throughout this paper unless specified otherwise.

II. GENERAL FORMULATION AND RESULTS FOR THE TWO-STATE TDER MODEL

In this Section we generalize the two-state TDER model, initially developed for a linearly polarized monochromatic field [54], to the general case of a laser pulse having an arbitrary waveform. As was found in Ref. [54], the use of the two-state model allows us to confirm that the factorized result for the HHG rate involves the *exact* TDER result for the photorecombination cross section (which is more accurate than the SFA result), at least for an initial s-state. This model also allows us to formulate the exact equations for the complex quasienergy for a system having a dynamical continuum and two bound states. Moreover, it allows us to extend the low-frequency (or adiabatic) approximation initially suggested in Ref. [70] (see also Refs. [81, 91]) to the case of HHG, whose amplitude can be related to the system's complex quasienergy [78].

The adiabatic approach requires an accurate choice of unperturbed wave functions for the active atomic electron. Indeed, if the initial state has nonzero angular momentum, then the wave functions for the magnetic sublevels can be mixed by an elliptically polarized laser field [17, 84] or by a two-color field with orthogonal linearly polarized components [16]. Since the case of nonzero angular momentum requires these special considerations, we shall restrict our considerations here to the simplest case of an initial s-state.

The two-state TDER model and the equations for the complex quasienergy are treated in Sec. II A. In Sec. II B we develop an adiabatic approximation for the complex quasienergy and derive adiabatic approximation expressions for the HHG amplitude for a driving laser field having an arbitrary spatial and temporal waveform. We discuss the relation of the present results to previous analytical results in Sec. II C.

A. Equations for the complex quasienergy

We shall analyse the complex quasienergy in a periodic laser field with a period $\mathcal{T}$ and corresponding frequency $\omega_\tau = 2\pi/\mathcal{T}$ within the framework of TDER theory [73, 74]. The TDER theory is based on the boundary condition for a quasistationary quasienergy wave function $\Phi_\epsilon(\boldsymbol{r}, t)$ [77, 116] formulated at small distances from the core [73, 74] (see Appendix A for details):

$$\begin{aligned}
&\iint \Phi_\epsilon(\boldsymbol{r}, t) Y^*_{l\,m}(\Omega) e^{in\omega_\tau t} d\Omega dt \\
&= f_n^{(l,m)} \left[\left(r^{-l-1} + \cdots \right) + \mathcal{B}_l(\epsilon + n\omega_\tau) \left(r^l + \cdots \right) \right], \quad (1) \\
&(2l-1)!!(2l+1)!!\mathcal{B}_l(\epsilon) = k^{2l+1} \cot\delta_l(k), \quad k = \sqrt{2\epsilon},
\end{aligned}$$

where ϵ is the complex quasienergy, $Y_{l\,m}(\Omega)$ is a spherical harmonic, $f_n^{(l,m)}$ is the Fourier-coefficient of a periodic function $f^{(l,m)}(t) = f^{(l,m)}(t + \mathcal{T}) = \sum_n f_n^{(l,m)} e^{-in\omega_\tau t}$ with period $\mathcal{T} = 2\pi/\omega_\tau$, and $\delta_l(k)$ is the scattering phase for the l-th angular momentum channel. A wave function satisfying boundary condition (1) can be composed from the partial wave functions, $\Phi_\epsilon^{(l,m)}(\boldsymbol{r}, t)$ [74]:

$$\begin{aligned}
\Phi_\epsilon^{(l,m)}(\boldsymbol{r}, t) &= -2\pi(-i)^l \int_{-\infty}^{t} e^{i\epsilon(t-t')} f^{(l,m)}(t') \\
&\times \mathcal{Y}_{l\,m} \left[\frac{\boldsymbol{r}}{t-t'} + \boldsymbol{K}'(t,t') \right] G(\boldsymbol{r}, t; 0, t') dt', \qquad (2)
\end{aligned}$$

$$\boldsymbol{K}'(t,t') = \boldsymbol{A}(t') - \frac{1}{t-t'} \int_{t'}^{t} \boldsymbol{A}(\xi) d\xi, \qquad (3)$$

where $G(\boldsymbol{r}, t; \boldsymbol{r}', t')$ is the retarded Green function for a free electron in a laser field with vector potential $\boldsymbol{A}(t)$ [116], and $\mathcal{Y}_{l\,m}(\boldsymbol{n})$ is a solid harmonic. In our analytical model we take into account only two phases $\delta_l(k)$ with $l = 0$ and $l = 1$. Equivalently, this means that our model atomic system has only two (s and p) bound states. Thus, the total wave function should be composed from the partial wave functions for $l = 0, 1$:

$$\Phi_\epsilon(\boldsymbol{r}, t) = \sum_{l=0,1} \sum_{m=-l}^{l} \Phi_\epsilon^{(l,m)}(\boldsymbol{r}, t). \qquad (4)$$

Expansions of partial wave functions with $l = 0$ and $l = 1$ at small distances have the form (cf. Ref. [74]):

$$\begin{aligned}
\Phi_\epsilon^{(0,0)}(\boldsymbol{r}, t) &\approx Y_{0,0}(\Omega) \sum_n \left(\frac{1}{r} + i\varkappa_n \right) f_n^{(0,0)} e^{-in\omega_\tau t} \\
&+ Y_{0,0}(\Omega) \int_{-\infty}^{t} \mathcal{G}'_\epsilon(t,t') f^{(0,0)}(t') dt' \\
&+ ir \sum_{\mu=-1}^{1} \frac{(-1)^\mu Y_{1,\mu}(\Omega)}{\sqrt{3}} \int_{-\infty}^{t} \mathcal{G}_\epsilon(t,t') \\
&\times f^{(0,0)}(t') K_{-\mu} dt', \qquad (5a)
\end{aligned}$$

$$\begin{aligned}
\Phi_\epsilon^{(1,m)}(\boldsymbol{r}, t) &\approx Y_{1,m}(\Omega) \sum_n \left(\frac{1}{r^2} + \frac{\varkappa_n^2}{2} + \frac{i\varkappa_n^3 r}{3} \right) \\
&\times f_n^{(1,m)} e^{-in\omega_\tau t} \\
&- iY_{0,0}(\Omega)\sqrt{3} \int_{-\infty}^{t} \mathcal{G}_\epsilon(t,t') f^{(1,m)}(t') K'_m dt' \\
&- irY_{1,m}(\Omega) \int_{-\infty}^{t} \frac{\mathcal{G}'_\epsilon(t,t') f^{(1,m)}(t')}{t-t'} dt' \\
&+ r \sum_{\mu=-1}^{1} (-1)^\mu Y_{1,\mu}(\Omega) \\
&\times \int_{-\infty}^{t} \mathcal{G}_\epsilon(t,t') f^{(1,m)}(t') K'_m K_{-\mu} dt', \qquad (5b)
\end{aligned}$$

$$\mathcal{G}'_\epsilon(t,t') = \frac{\left[e^{i\Delta(t,t')} - 1 \right] e^{i\epsilon(t-t')}}{\sqrt{2\pi i}(t-t')^{3/2}}, \qquad (5c)$$

$$\mathcal{G}_\epsilon(t,t') = \frac{e^{i\Delta(t,t') + i\epsilon(t-t')}}{\sqrt{2\pi i}(t-t')^{3/2}}, \qquad (5d)$$

$$\Delta(t,t') = -\frac{1}{2} \int_{t'}^{t} \left[\boldsymbol{A}(\xi) - \frac{1}{t-t'} \int_{t'}^{t} \boldsymbol{A}(\xi') d\xi' \right]^2 d\xi, \qquad (5e)$$

$$\boldsymbol{K}(t,t') = \boldsymbol{A}(t) - \frac{1}{t-t'} \int_{t'}^{t} \boldsymbol{A}(\xi) d\xi, \qquad (5f)$$

where $m = 0, \pm 1$, $\varkappa_n = \sqrt{2(\epsilon + n\omega_\tau)}$ (the square root is taken on the upper sheet of the Riemann surface), and K'_m, K_m are the circular components of vectors $\boldsymbol{K}'$ and $\boldsymbol{K}$, which are given by expressions $n_{\pm 1} = \mp(n_x \pm i n_y)/\sqrt{2}$, $n_0 = n_z$, where the vector $\boldsymbol{n}$ is either the vector $\boldsymbol{K}' \equiv \boldsymbol{K}'(t,t')$ or the vector $\boldsymbol{K} \equiv \boldsymbol{K}(t,t')$. It should be noted that the first terms in Eqs. (5a) and (5b) correspond to the first few terms of an expansion of the spherical Hankel function $h_l(i\varkappa_n r)$, which is the solution of the Schrödinger equation for a free electron with a given l and "energy" $\varkappa_n^2/2$ [43]. These terms are not affected by the laser field, while other (regular in r) terms of Eqs. (5a) and (5b) are laser-induced and tend to zero when the laser field is turned off.

By taking into account expansions (5a) and (5b), we match the wave function (4) to the boundary condition (1) and obtain equations for the complex quasienergy ϵ and the Fourier-coefficients $f_n^{(l,m)}$:

$$\begin{aligned}
&\left[\mathcal{B}_0(\epsilon + n\omega_\tau) - i\varkappa_n \right] f_n^{(0,0)} \\
&= \frac{1}{\mathcal{T}} \int_{-\mathcal{T}/2}^{\mathcal{T}/2} \int_{-\infty}^{t} \mathcal{G}'_\epsilon(t,t') f^{(0,0)}(t') e^{in\omega_\tau t} dt' dt \\
&- i\frac{\sqrt{3}}{\mathcal{T}} \sum_{m'} \int_{-\mathcal{T}/2}^{\mathcal{T}/2} \int_{-\infty}^{t} \mathcal{G}_\epsilon(t,t') f^{(1,m')}(t') K'_{m'} \\
&\times e^{in\omega_\tau t} dt' dt, \qquad (6a)
\end{aligned}$$

$$\left[\mathcal{B}_1(\epsilon+n\omega_\tau)-\frac{i\varkappa_n^3}{3}\right]f_n^{(1,m)}$$
$$=\frac{(-1)^m}{\mathcal{T}}\sum_{m'}\int\limits_{-\mathcal{T}/2}^{\mathcal{T}/2}\int\limits_{-\infty}^{t}\mathcal{G}_\epsilon(t,t')f^{(1,m')}(t')K'_{m'}K_{-m}$$
$$\times e^{in\omega_\tau t}dt'dt-\frac{i}{\mathcal{T}}\int\limits_{-\mathcal{T}/2}^{\mathcal{T}/2}\int\limits_{-\infty}^{t}\frac{\mathcal{G}'_\epsilon(t,t')}{(t-t')}f^{(1,m)}(t')e^{in\omega_\tau t}dt'dt$$
$$+i\frac{(-1)^m}{\sqrt{3}\mathcal{T}}\int\limits_{-\mathcal{T}/2}^{\mathcal{T}/2}\int\limits_{-\infty}^{t}\mathcal{G}_\epsilon(t,t')f^{(0,0)}(t')K_{-m}e^{in\omega_\tau t}dt'dt. \tag{6b}$$

Although Eqs. (6a) and (6b) are rather cumbersome, their solution is greatly simplified in the adiabatic approximation (see Refs. [70, 91, 117]). For simplicity, we do not consider the resonant case between two (s and p) atomic states, which requires detailed consideration. In the adiabatic approximation for an initial s-state, the Fourier-coefficients $f_n^{(0,0)}$ and $f_n^{(1,m)}$ can be obtained from Eqs. (6a) and (6b) by substituting on the right-hand sides of these equations $f^{(0,0)}(t)=f_0^{(0,0)}$ and $f^{(1,m)}(t)=0$:

$$f_n^{(0,0)}=\frac{f_0^{(0,0)}}{\mathcal{T}}\left[\mathcal{B}_0(\epsilon+n\omega_\tau)-i\varkappa_n\right]^{-1}$$
$$\times\int\limits_{-\mathcal{T}/2}^{\mathcal{T}/2}\int\limits_{-\infty}^{t}\mathcal{G}'_\epsilon(t,t')e^{in\omega_\tau t}dt'dt, \tag{7a}$$
$$f_n^{(1,m)}=\frac{i(-1)^m f_0^{(0,0)}}{\sqrt{3}\mathcal{T}}\left[\mathcal{B}_1(\epsilon+n\omega_\tau)-\frac{i\varkappa_n^3}{3}\right]^{-1}$$
$$\times\int\limits_{-\mathcal{T}/2}^{\mathcal{T}/2}\int\limits_{-\infty}^{t}\mathcal{G}_\epsilon(t,t')K_{-m}e^{in\omega_\tau t}dt'dt. \tag{7b}$$

For $n\neq 0$, $\mathcal{G}'_\epsilon(t,t')$ in the integrand of Eq. (7a) can be replaced by $\mathcal{G}_\epsilon(t,t')$.

B. Adiabatic approximation for the HHG amplitude in the TDER model

The HHG amplitude in a strong periodic laser field can be found as the first derivative of the complex quasienergy in a two-component field [78] equal to the sum of the strong periodic laser field and a weak (infinitesimal) harmonic field of frequency Ω with electric vector $\boldsymbol{F}_\Omega(t)=F_\Omega\mathrm{Re}[\boldsymbol{e}_\Omega e^{-i\Omega t}]$, where $\boldsymbol{e}_\Omega$ is the polarization vector. According to Ref. [78], the laser-induced dipole moment is given by expression

$$\boldsymbol{D}_\Omega=-4\frac{\partial\Delta\epsilon}{\partial\boldsymbol{F}^*_\Omega},\quad \boldsymbol{F}^*_\Omega=F_\Omega\boldsymbol{e}^*_\Omega, \tag{8}$$

where $\Delta\epsilon$ is linear in the F_Ω correction to the complex quasienergy of the target atom in the strong periodic laser field.

For a short laser pulse having an arbitrary waveform, the HHG amplitude can be found by replacing the isolated short pulse by a train of such short pulses, with the period of the train equal to $\mathcal{T}=2\pi/\omega_\tau$. In this case, the HHG amplitude, $\mathcal{A}(\Omega)$, can be found in the limit $\omega_\tau\to 0$ for fixed $\Omega=N\omega_\tau$ [80]:

$$\mathcal{A}(\Omega)=\boldsymbol{e}_\Omega{}^*\cdot\boldsymbol{D}(\Omega),\quad \boldsymbol{D}(\Omega)=\lim_{\omega_\tau\to 0}\boldsymbol{D}_\Omega/\omega_\tau. \tag{9}$$

The equation for the complex quasienergy ϵ in a strong periodic field and a weak harmonic field can be obtained from Eq. (6) by replacing $\boldsymbol{A}(t)\to\widetilde{\boldsymbol{A}}(t)$, where $\widetilde{\boldsymbol{A}}(t)$ is the vector potential of the two-component field,

$$\widetilde{\boldsymbol{A}}(t)=\boldsymbol{A}_\tau(t)+\frac{F_\Omega}{\Omega}\mathrm{Im}\left[\boldsymbol{e}_\Omega e^{-i\Omega t}\right], \tag{10}$$

and $\boldsymbol{A}_\tau(t)$ is the vector potential of the train of short pulses separated in time by $\mathcal{T}$.

The detailed calculation of $\Delta\epsilon$ in the TDER model is presented in Appendix B. Using that result, the result for $\boldsymbol{D}(\Omega)$ can be presented in the form:

$$\boldsymbol{D}(\Omega)=\boldsymbol{D}_1(\Omega)+\boldsymbol{D}_2(\Omega)+\boldsymbol{D}_3(\Omega), \tag{11}$$

where each term will now be discussed in turn.

The first term in Eq. (11) for the dipole has the form:

$$\boldsymbol{D}_1(\Omega)=\int_{-\infty}^{\infty}\boldsymbol{D}_1(t)e^{i\Omega t}dt, \tag{12}$$

$$\boldsymbol{D}_1(t)=-i\mathcal{C}g(\Omega)\int_{-\infty}^{t}\mathcal{G}_{-I_p}(t,t')\boldsymbol{K}(t,t')dt', \tag{13}$$

$$g(\Omega)=\frac{1}{2\Omega^2}+\frac{a(-\Omega)}{\mathcal{B}_1(-I_p+\Omega)-i\varkappa_\Omega^3/3},$$
$$a(-\Omega)=\frac{1}{2\Omega}\left[\kappa+i\frac{(2\Omega-2I_p)^{3/2}}{3\Omega}-\frac{\kappa^3}{3\Omega}\right],$$
$$\varkappa_\Omega=\sqrt{2(\Omega-I_p)},\quad \mathcal{C}=C_\kappa^2\kappa/\pi,$$

where the definition of $\boldsymbol{K}(t,t')$ is given by Eq. (5f), that of $\mathcal{G}_{-I_p}(t,t')$ by Eq. (5d), and $I_p=\kappa^2/2$ is the ionization potential.

The second term in Eq. (11) has the form:

$$\boldsymbol{D}_2(\Omega)=\int_{-\infty}^{\infty}\boldsymbol{D}_2(t)dt, \tag{14}$$

$$\boldsymbol{D}_2(t)=-i\frac{\mathcal{C}}{2\Omega^2}\int_{-\infty}^{t}\mathcal{G}_{-I_p}(t,t')\boldsymbol{K}'(t,t')e^{i\Omega t'}dt', \tag{15}$$

where $\boldsymbol{K}'(t,t')$ is defined in Eq. (3). For $\Omega\gg I_p\gg\omega$ (where ω is the carrier frequency of the driving laser pulse), the term $\boldsymbol{D}_2(t)$ is much smaller than $\boldsymbol{D}_1(t)$ and can be neglected. Indeed, since $I_p\gg\omega$, the integral in t' can be estimated using the saddle point method. The saddle points for the integral (15) are given by

$$\boldsymbol{K}'^2(t,t')=-2(I_p+\Omega), \tag{16}$$

while for the integral (13) they are given by the equation

$$\boldsymbol{K'}^2(t,t') = -2I_p. \tag{17}$$

Obviously, the solutions of Eq. (16) have larger imaginary parts than the corresponding solutions of Eq. (17), resulting in $\boldsymbol{D}_2(t)$ being exponentially small compared to $\boldsymbol{D}_1(t)$. Physically, the dipole $\boldsymbol{D}_2(\Omega)$ describes a suppressed harmonic generation channel in which the bound electron, instead of tunneling, emits a high-energy harmonic and then returns to the initial state by absorbing driving laser photons (cf. the discussion in Ref. [36]).

The third term in (11) can be presented as follows:

$$\boldsymbol{D}_3(\Omega) = \int_{-\infty}^{\infty} \boldsymbol{D}_3(t)dt, \tag{18}$$

$$\boldsymbol{D}_3(t) = -i\frac{\mathcal{C}}{2\Omega^2}\int\limits_{-\infty}^{t} \mathcal{G}_{-I_p}(t,t')\int_{t'}^{t}\boldsymbol{F}(\xi)e^{i\Omega\xi}d\xi dt', \tag{19}$$

where $\boldsymbol{F}(t) = -\partial\boldsymbol{A}(t)/\partial t$. The integral (19) is also small compared to the integral in Eq. (13) for $\Omega \gg I_p \gg \omega$. Indeed, if ω and F are the carrier frequency and the strength of the laser pulse, then $\boldsymbol{A}(t)$ is of the order of F/ω, while the integral over ξ in Eq. (19) is of the order of F/Ω. Thus $\boldsymbol{D}_3(\Omega)$ is Ω/ω times smaller than $\boldsymbol{D}_1(\Omega)$ for $\Omega \gg \omega$. Therefore, by analyzing the three terms in Eq. (11), we find that only $\boldsymbol{D}_1(\Omega)$ contributes in the case that $\Omega \gg I_p \gg \omega$, i.e., $\boldsymbol{D}(t) \approx \boldsymbol{D}_1(t)$.

The dipole moment $\boldsymbol{D}_1(\Omega)$ in Eq. (12) can be evaluated analytically in the adiabatic limit (as shown in Appendix C) and $\boldsymbol{D}(\Omega)$ can then be presented in the form:

$$\boldsymbol{D}(\Omega) = \sum_j \boldsymbol{d}_j. \tag{20}$$

Each partial sub-cycle dipole $\boldsymbol{d}_j$ is associated with a closed *real* trajectory, which starts at the moment t'_j and finishes at time t_j. Starting and returning times are given by solutions of a system of transcendental equations:

$$\boldsymbol{K}'_j \cdot \dot{\boldsymbol{K}}'_j = 0, \tag{21a}$$

$$\frac{\boldsymbol{K}_j^2}{2} = E - \Delta\mathcal{E}_j, \tag{21b}$$

$$\Delta\mathcal{E}_j = -\frac{\boldsymbol{K'}_j^2+\kappa^2}{2(t_j-t'_j)}\left[\frac{2\frac{\boldsymbol{K}_j\cdot\boldsymbol{K}'_j}{t-t'_j} - \boldsymbol{F}'_j\cdot(\boldsymbol{K}_j-\boldsymbol{K}'_j)}{\boldsymbol{F}'^2_j - \boldsymbol{K}'_j\cdot\dot{\boldsymbol{F}}'_j}\right],$$

where $\boldsymbol{K}'_j \equiv \boldsymbol{K}'(t_j,t'_j)$, $\dot{\boldsymbol{K}}'_j \equiv \partial\boldsymbol{K}'(t_j,t'_j)/\partial t'_j$, $\boldsymbol{K}_j \equiv \boldsymbol{K}(t_j,t'_j)$, $\boldsymbol{F}'_j \equiv \boldsymbol{F}(t'_j)$, and $\dot{\boldsymbol{F}}'_j \equiv \dot{\boldsymbol{F}}(t'_j)$. Equation (21a) shows that at the starting time t'_j the kinetic energy of the electron in the laser field is minimal, while Eq. (21b) ensures that at the moment of return the electron has kinetic energy $E - \Delta\mathcal{E}_j$. The sub-cycle dipole can be presented in a factorized form:

$$\boldsymbol{d}_j = a_j^{(\mathrm{tun})}\boldsymbol{a}_j^{(\mathrm{prop})}f_{\mathrm{rec}}(E), \tag{22}$$

where each of the three factors is discussed below.

The *tunneling ionization* factor, $a_j^{(\mathrm{tun})}$, is given by the detachment amplitude in the adiabatic approximation [51, 118] [see Eq. (13) in Ref. [51]]:

$$a_j^{(\mathrm{tun})} = \frac{C_\kappa}{\pi}\sqrt{\frac{\kappa}{2}}\frac{e^{-\frac{\varkappa_j^3}{3\mathcal{F}_j}}}{\sqrt{\varkappa_j\mathcal{F}_j}}e^{i\mathcal{S}(\boldsymbol{p}_j,t'_j)}, \tag{23}$$

where

$$\mathcal{F}_j = \sqrt{\boldsymbol{F'}^2_j - \boldsymbol{K}'_j\cdot\dot{\boldsymbol{F}}'_j}, \quad \varkappa_j = \sqrt{2I_p + \boldsymbol{K'}^2_j},$$

$$\mathcal{S}(\boldsymbol{p},t) = \int_{-\infty}^{t}\left\{\frac{1}{2}\left[\boldsymbol{p}+\boldsymbol{A}(t')\right]^2 + I_p\right\}dt',$$

$$\boldsymbol{p}_j = -\frac{1}{t_j-t'_j}\int_{t'_j}^{t_j}\boldsymbol{A}(\xi)d\xi.$$

The factor $a_j^{(\mathrm{tun})}$ describes the ionization step in the three-step scenario of HHG [45].

The *propagation* factor, $\boldsymbol{a}_j^{(\mathrm{prop})}$, is given by the expression:

$$\boldsymbol{a}_j^{(\mathrm{prop})} = i\frac{e^{-i\mathcal{S}(\boldsymbol{p}_j,t_j)+i\Omega t_j}\hat{\boldsymbol{k}}_j}{(t_j-{t'}_j)^{3/2}\sqrt{\boldsymbol{K}_j\cdot\dot{\boldsymbol{K}}_j}}, \tag{24}$$

where $\hat{\boldsymbol{k}}_j = \boldsymbol{K}_j/\sqrt{2E}$. This factor describes the propagation of the EWP in the continuum from the moment of ionization, t'_j, to the moment of recombination, t_j.

The last factor in $\boldsymbol{d}_j$, $f_{\mathrm{rec}}(E)$, is the *exact amplitude for radiative recombination* to the ground state with $l = 0$ in the two-state TDER model for the electron with wave vector $\boldsymbol{k}$ ($k = \sqrt{2E}$), whose direction coincides with the polarization vector of the emitted linearly polarized photon [54]:

$$f_{\mathrm{rec}}(E) = iC_\kappa\frac{4k\sqrt{\pi\kappa}}{(k^2+\kappa^2)^2} \times\left[1 - \frac{i}{4\widetilde{k}^3}\left(1-2i\widetilde{k}\right)\left(1+i\widetilde{k}\right)^2\left(e^{2i\delta_1(k)}-1\right)\right]. \tag{25}$$

where $\widetilde{k} = k/\kappa$. [Note that if one neglects the scattering phase, i.e., if one sets $\delta_1(k) = 0$, the result (25) reduces to that in the Born approximation (cf. Ref. [54]).]

The analytic approach developed above does not take into account depletion of the ground state due to tunneling ionization. To overcome this limitation, we introduce the depletion factor, $\mathcal{P}_j$, for each partial dipole $\boldsymbol{d}_j$:

$$\mathcal{P}_j = \exp\left[-\frac{1}{2}\int_{-\infty}^{t'_j}\Gamma(F(t))dt - \frac{1}{2}\int_{-\infty}^{t_j}\Gamma(F(t))dt\right], \tag{26}$$

where $\Gamma(F)$ is the detachment rate for the initial state in a DC field with strength F. This factor describes depletion effects at the moment of ionization and recombination in the adiabatic limit [81]. Taking into account the depletion factor, $\boldsymbol{D}(\Omega)$ has the form:

$$\boldsymbol{D}(\Omega) = \sum_j \mathcal{P}_j \boldsymbol{d}_j. \tag{27}$$

With given $\boldsymbol{D}(\Omega)$, the dimensionless spectral density of the emitted radiation is given by (see, e.g., Ref. [80]):

$$\rho(\Omega) = \frac{\Omega^4}{4c^3} \left|\boldsymbol{D}(\Omega)\right|^2, \tag{28}$$

where $c \approx 137$ is the speed of light. Substituting the explicit form of the dipole moment (27) into Eq. (28) and taking into account that

$$\sigma_{\rm rec}(E) = \frac{\Omega^3}{2\pi k c^3} |f_{\rm rec}(E)|^2, \tag{29}$$

we obtain the spectral density $\rho(\Omega)$ in the form:

$$\rho(\Omega) = W(E)\sigma_{\rm rec}(E), \quad \Omega = E + I_p, \tag{30}$$

where $W(E)$ is the EWP. The explicit form of $W(E)$ is obvious from Eqs. (28) and (29):

$$W(E) = \frac{\pi}{2}\Omega k \left| \sum_j \mathcal{P}_j a_j^{(\rm tun)} \boldsymbol{a}_j^{(\rm prop)} \right|^2. \tag{31}$$

We note that the result (30) is applicable for $\Omega \gg I_p$.

C. Connection with alternative analytic approaches and studies

1. Quantum orbits approach

The workhorse for treating strong field phenomena is the QOA [34, 39, 41]. In the framework of this approach, the HHG amplitude is presented as a sum of partial amplitudes, each of which is associated with a closed complex electron trajectory in the laser field. Although these trajectories are associated with complex times, they still satisfy classical Newton equations. The complex closed trajectories are determined by their starting (t') and returning (t) times, which are the solutions of the system of equations [34, 39, 41]:

$$\boldsymbol{K}'^2(t,t') = -\kappa^2, \tag{32a}$$
$$\boldsymbol{K}^2(t,t') = 2E. \tag{32b}$$

As shown in Ref. [119], in the limit $\mathrm{Im}\,\omega t' \ll 1$ the solution of the system of equations (32) reduces to the solution of the system of equations (21). Thus, the present approach is a limiting case of the more general QOA.

However, in contrast to the quantum orbits theory, the present approach associates partial HHG amplitudes with classical (real-valued) closed trajectories. These simplify the classical interpretation of HHG as well as the numerical issues associated with finding the contributing trajectories: the solutions of Eq. (21) together with Eq. (C11) may be used as a starting guess for the solutions of the system (32). In the tunneling regime, they almost match the solution of Eq. (32) (for details, see Ref. [119]).

2. Analytic expansion of the HHG amplitude in terms of extreme trajectories

The analysis of *real* classical trajectories shows that near some energies $E \approx E_{\rm max}^{(k)}$ two classical trajectories coalesce into one [120–122]. This coalescence results in a singularity in the harmonic spectral density that is known as a caustic. The occurrence of this caustic results from the fact that high-order derivatives (in time t) of the action $S(t,t')$ approach zero near the energies $E = E_{\rm max}^{(k)}$ [120–122]. In the simplest case, the condition for appearance of a caustic is that the second-order derivative (with respect to t) of the classical action $S(t,t')$ is zero, i.e., it coincides with the condition for an extremum of the energy gained by the electron in the laser field.

As shown in Refs. [80, 83, 123], the HHG amplitude can also be presented as a sum of partial amplitudes, each associated with an extreme trajectory in which the electron returns to the origin with energy $E_{\rm max}^{(k)}$. For a linearly polarized field, the electron propagates in the continuum with zero initial momentum and the extremum in the energy gained is given by the zero of the derivative of the vector $\boldsymbol{K}(t,t')$ with respect to time t:

$$\boldsymbol{K}'(t,t') = 0, \tag{33a}$$
$$\frac{\partial \boldsymbol{K}(t,t')}{\partial t} = 0. \tag{33b}$$

Expanding solutions of Eq. (21) near the roots of Eq. (33) (which do not depend on the energy E), it can be shown (see details in Appendix D) that expansion of the HHG amplitude in terms of extreme trajectories coincides asymptotically (in an energy region not too close to caustics) with the results of the present approach.

III. EXTENSION TO THE CASE OF NEUTRAL ATOMS HAVING AN ACTIVE s-ELECTRON

The Coulomb field changes the laser-induced electron dynamics significantly. Even though the analytical description of these effects is challenging, the low-frequency (adiabatic) regime allows for simplifications. Our result for $\boldsymbol{D}(\Omega)$ [see Eqs. (20) and (22)] was obtained within an analytical model that supports two nonzero scattering phases with $l = 0$ and $l = 1$. Equivalently, this means that the electron moves in a short-range potential supporting two bound states. Within this model, we derived (for the case of a short driving laser pulse having an arbitrary waveform) the factorization of the HHG yield in terms of an EWP and the *exact* recombination cross section for this two-bound-state system. This result suggests an appropriate extension of the result for $\boldsymbol{D}(\Omega)$ to the case of an atom whose active electron, in an initial s-state, experiences a long-range Coulomb potential. The extension consists, first, in simply replacing the model-dependent photorecombination cross section factor, $\sigma_{\rm rec}(E)$, in Eq. (30) with its atomic counterpart, which properly takes into account the atomic dynamics in a Coulomb field relevant to the recombination process. Second (and less simple), one must also introduce appropriate Coulomb corrections to the EWP factor, $W(E)$, in Eq. (30).

In the low-frequency (adiabatic) limit, the influence of the Coulomb potential on the EWP factor can be taken into account by introducing quasiclassical Coulomb factors [44, 51, 124–126]. The Coulomb correction for the EWP factor of the HHG amplitude was discussed briefly in Sec. V of Ref. [51]. It was argued there that, to a good approximation, this Coulomb correction can be introduced only in the ionization factor. (A more detailed analysis of the Coulomb phase corrections for the HHG amplitude in the quasiclassical approximation was discussed recently in Ref. [52].) Therefore, we modify the ionization factor (23) by multiplying it by the Coulomb correction Q_j [51]:

$$Q_j = Q_{\rm stat}^{(j)} R^{(j)}, \tag{34}$$

$$Q_{\rm stat}^{(j)} = \left(\frac{2\kappa^3}{F'_j}\right)^{Z/\kappa}, \quad F'_j = \sqrt{\boldsymbol{F'}^2_j},$$

$$R_j = \left[\frac{2F'_j}{\mathcal{F}_j\left(\sqrt{1+\dfrac{\boldsymbol{K}'^2_j}{\kappa^2}}+\dfrac{2}{\sqrt{3}}\sqrt{1-\dfrac{\boldsymbol{F}'^2_j}{4\mathcal{F}^2_j}}\right)}\right]^{Z/\kappa},$$

where Z is the charge of the residual atomic core (where $Z=0$ and 1 for negative ions and neutral atoms, respectively).

Thus, in the case of neutral atoms, the total and partial dipole moments become [109]:

$$\boldsymbol{D}(\Omega) = \sum_j \mathcal{P}_j \boldsymbol{d}_j, \quad \boldsymbol{d}_j = Q_j a_j^{\rm (tun)} \boldsymbol{a}_j^{\rm (prop)} f_{\rm rec}(E), \tag{35}$$

where $f_{\rm rec}(E)$ is the *exact* photorecombination amplitude. For calculating $\mathcal{P}_j$ we use the expression for the decay rate in a DC field [127]. The form (35) of the partial dipole moment agrees with previous parametrizations of the HHG yield in terms of the EWP and the photorecombination cross section [53, 54, 82, 83, 87]. The accuracy of this extension to the case of a laser pulse having an arbitrary waveform is discussed in Sec. IV B.

IV. RESULTS FOR HHG IN BICIRCULAR FIELDS WITH OPPOSITE HELICITIES

We present here the application of the general theory presented above to HHG in bicircular driving laser fields. In Sec. IV A we consider the case of long bicircular driving laser pulses. In Sec. IV B we compare our analytical results for the case of short bicircular driving laser pulses with results of numerical solutions of the 3D TDSE. In Sec. IV C we provide a trajectory analysis of our analytical results. Finally, in Sec. IV D we develop (and present the physical basis for) a two-dipole model of HHG emission that provides a clear explanation of our short, bicircular pulse HHG results and indicates a means for controlling the polarization of the harmonics.

A. Bicircular field with monochromatic components

We consider here the case in which both components of the bicircular field are long pulses. They have frequencies ω and 2ω and polarization vectors $\boldsymbol{e}_\omega = (\boldsymbol{e}_x + i\boldsymbol{e}_y)/\sqrt{2}$ and $\boldsymbol{e}_{2\omega} = (\boldsymbol{e}_x - i\boldsymbol{e}_y)/\sqrt{2}$. The electric field when the two components have equal amplitudes, F, is

$$\boldsymbol{F}(t) = F[{\rm Re}(\boldsymbol{e}_\omega e^{-i\omega t}) + {\rm Re}(\boldsymbol{e}_{2\omega} e^{-2i\omega t})]. \tag{36}$$

For circularly polarized components with opposite helicities we have $\boldsymbol{e}_{2\omega}\cdot\boldsymbol{e}_\omega = 1$ and $\boldsymbol{e}_{2\omega}\cdot\boldsymbol{e}_{2\omega} = \boldsymbol{e}_\omega\cdot\boldsymbol{e}_\omega = \boldsymbol{e}^*_{2\omega}\cdot\boldsymbol{e}_\omega = \boldsymbol{e}_{2\omega}\cdot\boldsymbol{e}^*_\omega = 0$. Angular momentum and parity conservation selection rules require that the generated harmonics have energies $(3n+1)\omega$ or $(3n-1)\omega$ and that harmonics with the energy $3n\omega$ are forbidden [94, 95, 106, 128]. These selection rules become particularly transparent when one notes that the magnetic quantum number, m_l, of the electron remains unchanged after absorbing a pair of circularly polarized photons with opposite helicities (with polarization vectors $\boldsymbol{e}_\omega$ and $\boldsymbol{e}_{2\omega}$), i.e., after absorbing the energy 3ω. Also, in order for the electron to recombine with the atom (in its initial s-state) by emitting a harmonic photon, one must have $m_l = \pm 1$, i.e., the active electron must absorb either one more or one less photon of energy ω as compared to the number of photons absorbed with energy 2ω.

These general results can also be obtained from the analytical expression (20) for the dipole $\boldsymbol{D}(\Omega)$ (i.e., neglecting depletion effects). Indeed, owing to the temporal symmetry of the laser field, Eq. (21) is invariant with respect to the substitutions: $t' \to t' + nT/3$ and $t \to t + nT/3$, where $T = 2\pi/\omega$ and n is an integer. Thus, all joint solutions of Eq. (21) can be reduced to the "fundamental" solutions $\{t_{0,j}, t'_{0,j}\}$, so that $t'_j = t'_{0,j} + \nu T/3$, $t_j = t_{0,j} + \nu T/3$, where ν is an integer number. Fundamental solutions can be defined by setting an additional condition for $t'_{0,j}$ or $t_{0,j}$: e.g., $t'_{0,j} \in (0, T/3)$ with $\nu = 0$. Obviously, under these substitutions all scalars, which define $\boldsymbol{D}(\Omega)$ in Eq. (35), remain unchanged.

In order to establish the symmetry relation for the vector $\hat{\boldsymbol{k}}_j = \boldsymbol{K}(t_j, t_j')/\sqrt{2E}$, we present this vector as a sum of two vectors:

$$\hat{\boldsymbol{k}}_j = \hat{\boldsymbol{k}}_j^{(\omega)} + \hat{\boldsymbol{k}}_j^{(2\omega)}, \tag{37}$$

where [cf. Eq. (5f)]

$$\hat{\boldsymbol{k}}_j^{(l\omega)} = \frac{1}{\sqrt{2E}} \left(\boldsymbol{A}_l(t_j) - \frac{\int_{t'_j}^{t_j} \boldsymbol{A}_l(\xi) d\xi}{t_j - t'_j} \right), \tag{38}$$

and $\boldsymbol{A}_l(t)$ is the vector potential corresponding to the field component with frequency $l\omega$ ($l = 1, 2$). It can be explicitly confirmed that

$$\left(\hat{\boldsymbol{k}}_j^{(\omega)}\right)_\pm = e^{\pm \frac{2i\pi}{3}\nu} \left(\hat{\boldsymbol{k}}_{0,j}^{(\omega)}\right)_\pm, \tag{39a}$$

$$\left(\hat{\boldsymbol{k}}_j^{(2\omega)}\right)_\pm = e^{\mp \frac{4i\pi}{3}\nu} \left(\hat{\boldsymbol{k}}_{0,j}^{(2\omega)}\right)_\pm, \tag{39b}$$

where $\hat{\boldsymbol{k}}_{0,j}^{(l\omega)}$ are vectors $\hat{\boldsymbol{k}}_j^{(l\omega)}$ calculated with the substitutions $t_j \to t_{0,j}$, $t_j' \to t_{0,j}'$. Taking into account the symmetry relations (39), we obtain for the $\pm$-components of the vector $\hat{\boldsymbol{k}}_j$ a more complex symmetry relation:

$$\left(\hat{\boldsymbol{k}}_j\right)_\pm = e^{\pm i \frac{2\pi}{3}\nu} \left(\boldsymbol{k}_{0,j}^{(\omega)}\right)_\pm + e^{\mp i \frac{4\pi}{3}\nu} \left(\boldsymbol{k}_{0,j}^{(2\omega)}\right)_\pm. \tag{40}$$

Taking into account the invariance of the scalars and the symmetry relations (39), we can present the $\pm$-components of the vector $\boldsymbol{D}(\Omega)$ in the form:

$$\boldsymbol{D}_\pm(\Omega) = \sum_j \left(\boldsymbol{d}_{0,j} \cdot \hat{\boldsymbol{k}}_{0,j}\right) \left[\left(\hat{\boldsymbol{k}}_{0,j}^{(\omega)}\right)_\pm \sum_\nu e^{i\frac{2\pi\nu}{3}\left(\frac{\Omega}{\omega} \pm 1\right)} + \left(\hat{\boldsymbol{k}}_{0,j}^{(2\omega)}\right)_\pm \sum_\nu e^{i\frac{2\pi\nu}{3}\left(\frac{\Omega}{\omega} \mp 2\right)} \right], \tag{41}$$

where $\hat{\boldsymbol{d}}_{0,j}$ are vectors $\hat{\boldsymbol{d}}_j$ calculated with the substitutions $t_j \to t_{0,j}$, $t_j' \to t_{0,j}'$. Summation over ν in Eq. (41) can be performed analytically based on the relations:

$$f(N; x) = \sum_{\nu=-N}^{N} e^{i\frac{2\pi\nu}{3}x} = \frac{\sin\left[(2N+1)\frac{\pi x}{3}\right]}{\sin\left(\frac{\pi x}{3}\right)}, \tag{42a}$$

$$\lim_{N\to\infty} f(N; x) = 3 \sum_n \delta(x - 3n) \tag{42b}$$

and the dipole (41) can be presented in the final form:

$$\boldsymbol{D}_\pm(\Omega) = 3\omega\delta[\Omega - (3n \mp 1)\omega] \times \sum_j \left(\boldsymbol{d}_{0,j} \cdot \hat{\boldsymbol{k}}_{0,j}\right) \left(\hat{\boldsymbol{k}}_{0,j}\right)_\pm. \tag{43}$$

Equation (43) explicitly shows the orders of allowed harmonics and also that each harmonic has only one nonzero cyclic component (plus or minus), which indicates that the emitted harmonic is circularly polarized and that the two nearest harmonics have opposite helicities.

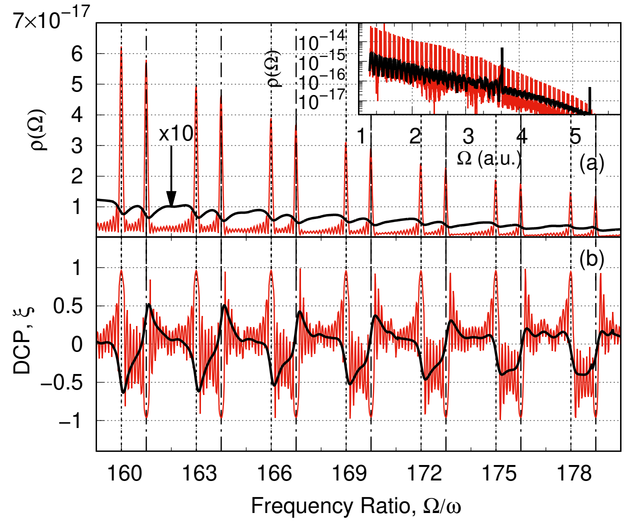

Figure 1. Analytically calculated HHG spectrum (a) and the degree of circular polarization (b) for the hydrogen atom interacting with a long $\omega - 2\omega$ bicircular field, with oppositely polarized components, the same peak intensity, $I = 10^{14}\,\mathrm{W/cm^2}$, $\lambda = 2\pi c/\omega = 1.6$ μm, and a trapezoidal envelope with a total duration of 10 optical cycles of the fundamental and 1 optical cycle linear turn-on and turn-off. *Thick solid (black) lines*: analytic results with depletion included; *thin solid (red) lines*: analytic results without depletion. The inset figure in (a) shows the shape of the HHG spectrum on a wide energy scale.

Note that ionization of an atomic system in a long laser pulse may play a crucial role in forming HHG peaks. Indeed, when depletion is significant, the depletion factor $\mathcal{P}_j$ affects the constructive or destructive interference in the coherent summation of partial dipoles generated during successive ionization bursts, thereby washing out the sharp peak structure at the allowed energies $\Omega = (3n \pm 1)\omega$ in the HHG spectrum (see Fig. 1).

To model the bicircular field with two monochromatic components, we consider in our analytical calculations two circularly polarized pulses with trapezoidal envelopes, with linear turn-on and turn-off in one optical period of the fundamental ($T_{\rm on,off} = 2\pi/\omega$), and a total duration of 10 fundamental cycles ($T_{\rm tot} = 10\times 2\pi/\omega$) with constant peak intensity. In Fig. 1 we present both HHG spectra and the degree of circular polarization [129, 130], ξ, of the harmonics calculated both with and without inclusion of depletion effects:

$$\xi = -2\frac{\mathrm{Im}\left[D_x(\Omega) D_y^*(\Omega)\right]}{|D_x(\Omega)|^2 + |D_y(\Omega)|^2}. \tag{44}$$

Our analytical results in Fig. 1 without inclusion of depletion effects explicitly show sharp peaks at the energies $\Omega = (3n \mp 1)\omega$, for which the degree of circular polarization is ± 1. These results are in agreement with previous studies [94, 95] and with the above discussion. The analytic results in Fig. 1 with inclusion of depletion clearly show the broadening and shifting of the HHG peaks as

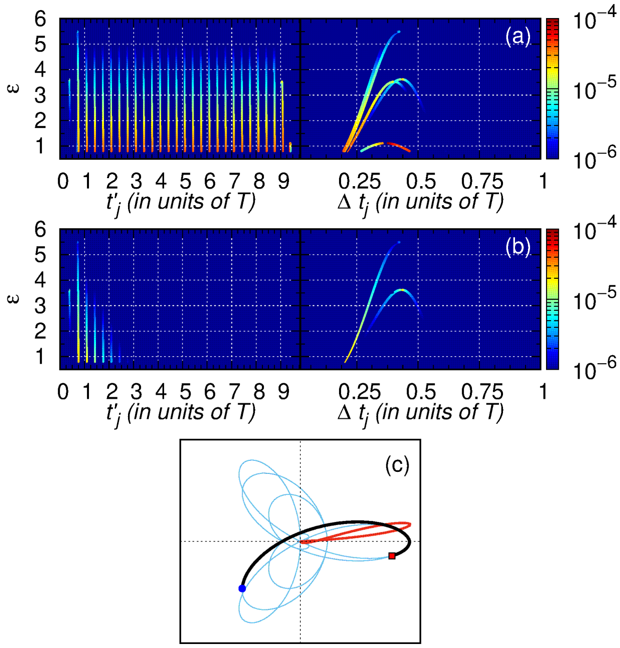

Figure 2. Dependence of the scaled return energy, $\varepsilon = E/u_p$, where $u_p = F^2/(4\omega^2)$, on the jth trajectory's ionization time, t'_j, and travel time, Δt_j. *Panel (a)*: results for the no depletion case; *panel (b)*: results including depletion. The laser parameters are the same as in Fig. 1. The color scale shows the relative contributions of the dipoles, $\propto |\boldsymbol{d}_j|$. *Panel (c)*: sketch of the dominant closed classical trajectory for $\Omega = I_p + 4u_p$ (red line beginning and ending at the origin with the electron moving counterclockwise) together with the corresponding electric field trajectory (black line) drawn from ionization (blue circle) to recombination (red square). The thin blue line shows the electric field trajectory for the entire pulse.

well as the changed polarization properties of the emitted harmonics.

In order to clarify the origin of these changes, we plot in Fig. 2 the dependence of the return energy on the ionization (t'_j) and the travel ($\Delta t_j = t_j - t'_j$) times both without (in panel a) and with (in panel b) depletion effects. In each optical cycle there are three ionization bursts. The properties of the laser-induced electron trajectories generated during the flat-top part of the laser pulse are the same from burst to burst [see the shape of the trajectory in Fig. 2 (c)]. The constructive interference of their contributions results in the sharp peaks in the HHG spectra when depletion is ignored. Trajectories born during the turn-on and turn-off of the pulse have slightly different ionization and recombination times, for the same harmonic number, but their contributions are not significant.

The main contribution to the HHG spectrum comes from the short trajectories with small travel times $\Delta t_j < T/2$, where $T = 2\pi/\omega$. With inclusion of the depletion effects, the partial dipoles $\boldsymbol{d}_j$ are unchanged, but their contributions are now governed by the factors $\mathcal{P}_j$. These factors gradually suppress the contributions of the partial dipoles $\boldsymbol{d}_j$ that correspond to larger ionization times [see Fig. 2 (b)]. Thus, only a few partial dipoles with unequal contributions determine the dipole $\boldsymbol{D}(\Omega)$. The small number of unequally-weighted partial dipoles leads to the broad "peaks" in the HHG spectra and changes the polarization properties of the harmonics (including even polarization reversals) [see Fig. 1(b)].

B. Comparison of adiabatic approximation and numerical TDSE results

To check the accuracy of our extension of the TDER model to the case of neutral atoms, we have compared our analytical results [obtained using Eqs. (28), (20), and (35)] with the numerically calculated HHG spectra obtained by solving the 3D TDSE:

$$i\frac{\partial\psi(\boldsymbol{r},t)}{\partial t} = \left[-\frac{\nabla^2}{2} + U(r) + \boldsymbol{r}\cdot\boldsymbol{F}(t)\right]\psi(\boldsymbol{r},t), \qquad (45)$$

where $\boldsymbol{F}(t)$ is the electric field of the laser pulse and $U(r)$ is the atomic potential. To avoid the Coulomb singularity at the origin and to obtain faster convergence of the numerical simulations at rather long wavelengths, we have used a smoothed Coulomb potential:

$$U(r) = -\frac{1}{r}\left[\tanh(r/a) + (r/b)\mathrm{sech}^2(r/a)\right], \qquad (46)$$

where $a = 0.3$ and $b = 0.46$. The values of a, b ensure that the energy of the ground state of the potential $U(r)$ coincides with that of atomic hydrogen. Moreover, the potential (46) provides similar behavior of the photoionization (or photorecombination) cross section from an initial s-state as for the bare Coulomb potential. The spectral density, $\rho(\Omega)$, is calculated as the Fourier-transform of the laser-induced dipole acceleration $\boldsymbol{a}(t)$:

$$\rho(\Omega) = \frac{|\boldsymbol{a}(\Omega)|^2}{4c^3}, \quad \boldsymbol{a}(\Omega) = \int_{-\infty}^{\infty} e^{i\Omega t}\boldsymbol{a}(t)dt, \qquad (47)$$

where

$$\boldsymbol{a}(t) = -\boldsymbol{F}(t) - \langle\psi|\nabla U(r)|\psi\rangle. \qquad (48)$$

The electric field was parameterized in terms of the integral of the vector potential, $\boldsymbol{R}(t)$, as follows:

$$\boldsymbol{F}(t) = -\frac{\partial \boldsymbol{A}(t)}{\partial t}, \quad \boldsymbol{A}(t) = \frac{\partial \boldsymbol{R}(t)}{\partial t}, \qquad (49a)$$

$$\boldsymbol{R}(t) = \boldsymbol{R}_1(t) + \boldsymbol{R}_2(t - T_{\mathrm{d}}), \qquad (49b)$$

$$\boldsymbol{R}_i(t) = \frac{F}{\omega_i^2} f_i(t)(\boldsymbol{e}_x\cos\omega_i t + \eta_i \boldsymbol{e}_y \sin\omega_i t), \qquad (49c)$$

$$f_i(t) = e^{-2\ln 2\, t^2/\tau_i^2} \qquad (49d)$$

where each component $i = 1, 2$ of the field $\boldsymbol{F}(t)$ has intensity F, carrier frequency ω_i ($\omega_1 = \omega_2/2 \equiv \omega$), ellipticity η_i ($\eta_1 = -\eta_2 = 1$), duration $\tau_i = 2\pi N_i/\omega$ (full width at

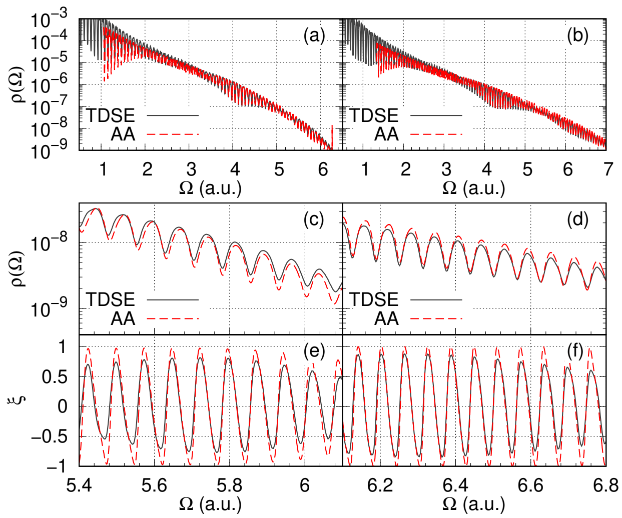

Figure 3. Comparison of TDSE and adiabatic approximation (AA) results [see Eq. (35)] for the HHG spectral density, $\rho(\Omega)$, of the H atom, on both large (a,b) and fine (c,d) energy scales, and for the degree of circular polarization, ξ, of the harmonics (e,f) for two different bicircular driving laser fields (49). For each field the peak intensity for both components is $I = cF^2/(8\pi) = 10^{14}\mathrm{W/cm}^2$, $\omega_1 = \omega_2/2 = \omega$, and the number of cycles is $N_1 = N_2 = 3$, with time delay $T_\mathrm{d} = 0$. Results in panels (a,c,e) are for $\lambda = 2\pi c/\omega = 1.8$ μm and those in panels (b,d,f) are for $\lambda = 2.2$ μm. *Solid (black) lines*: TDSE results; *dashed (red) lines*: AA results.

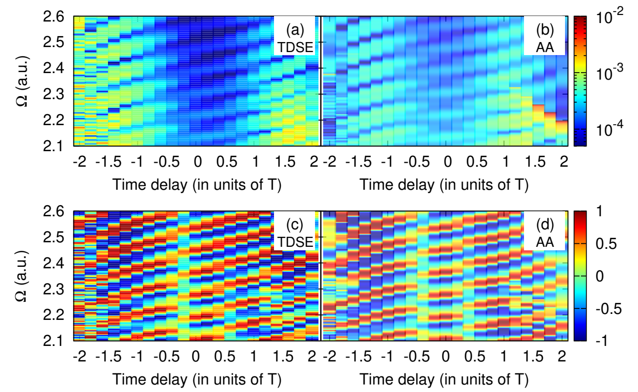

Figure 4. Comparison of TDSE and adiabatic approximation (AA) color-coded results for the H atom HHG spectral density, $\rho(\Omega)$, (a,b) and degree of circular polarization, ξ, (c,d) for a bicircular field (49) with peak intensity $I = 10^{14}\mathrm{W/cm}^2$ for each component, $\omega_1 = \omega_2/2 = \omega$, $N_1 = N_2 = 3$ cycles, and $\lambda = 2\pi c/\omega = 1.6$ μm plotted as a function of the two-color time delay T_d (in units of $T = 2\pi/\omega$) and the harmonic energy Ω. *Panels (a) and (c)*: TDSE results; *panels (b) and (d)*: AA results, which were plotted with the same resolution as the numerical TDSE results.

half maximum of the intensity), and number of cycles N_i. Also, in Eq. (49b) T_d is the time delay between the two components, with a negative time delay indicating that the 2ω-pulse precedes the ω-pulse.

To solve the TDSE numerically, we employ a split-step method based upon a fast Fourier-transform along the Cartesian coordinates x, y, and z [16, 17]. The use of Cartesian coordinates is because of the lack of spatial symmetry in the problem. For an atomic system in a strong MIR field, the numerical solution requires a large spatial grid owing to the large excursion amplitude of the electron motion, $\propto F/\omega^2$. For an intensity $I = 10^{14}$ W/cm^2, the simulations for $\lambda = 1.6$ μm and $\lambda = 1.8$ μm require for convergence $N_x = N_y = 1024$ (the number of grid points in x and y), and for $\lambda = 2.2$ μm and $\lambda = 2.4$ μm they require $N_x = N_y = 2048$. For the z-axis, the number of grid points is $N_z = 256$. The temporal and spatial steps were chosen to ensure convergence of the numerical results: $\Delta t = 0.025$ a.u., $\Delta x = \Delta y = \Delta z = 0.325$ a.u. The absorbing boundaries (using the method in Ref. [131]) have a width of 30 a.u. in the x and y directions and 15 a.u. in the z direction.

In Figs. 3-5 we compare numerical TDSE and adiabatic approximation results. We find excellent agreement for the high-energy parts of the HHG spectra, for which the adiabatic approximation is justified. For harmonic energies close to the ionization potential, we observe discrepancies owing to the contributions of terms that were omitted in the adiabatic approximation (see the discussion in Sec. II B).

We list here some key observations from the TDSE and adiabatic approximation results presented in Figs. 1 and 3-5:

(i) In contrast to the case of linear polarization, HHG spectra for bicircular fields do not show well-pronounced plateau structures with abrupt cutoffs [see the inset figure in Fig. 1(a) and Figs. 3(a) and 3(b)].

(ii) Both the HHG yield and the degree of circular polarization exhibit an oscillatory dependence on the time delay between the fundamental and the second harmonic, which can be exploited to control the polarization of the generated harmonic radiation (see Fig. 4).

(iii) For a fixed time delay, the HHG spectrum does not exhibit sharp peaks at $\Omega = (3n \pm 1)\omega$; the oscillatory structure can be tuned by the two-color time delay, leading to the emergence of seemingly forbidden harmonics with $\Omega = 3n\omega$ (see Figs. 3 and 5).

(iv) There is no symmetry in the HHG yield or in the polarization properties with respect to positive versus negative two-color time delays (see Figs. 4 and 5).

C. Trajectory analysis

As numerical solutions of the TDSE for MIR wavelengths are prohibitively expensive and not very flexible for detailed analyses, we carry out a trajectory analysis using the adiabatic approximation instead. The key quantities are the ionization and recombination times satisfying Eq. (21).

Our trajectory analysis starts with Eq. (21a), which we solve with respect to the ionization time, t'_j, considering

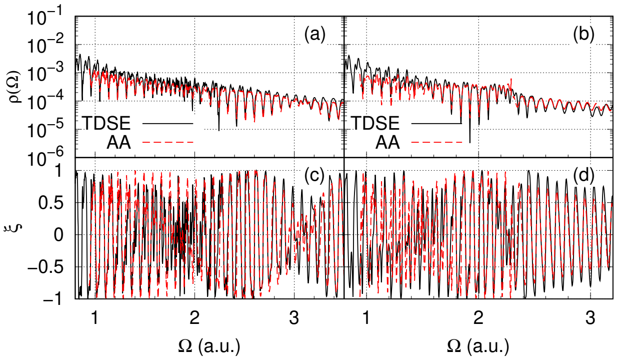

Figure 5. Cuts of HHG spectral density, $\rho(\Omega)$, and degree of circular polarization, ξ, from Fig. 4 for positive and negative time delays. *Panels (a,c)*: $T_{\rm d} = -1.4T$; *panels (b,d)*: $T_{\rm d} = 1.4T$. *Solid (black) lines*: TDSE results; *Dashed (red) lines*: adiabatic approximation (AA) results.

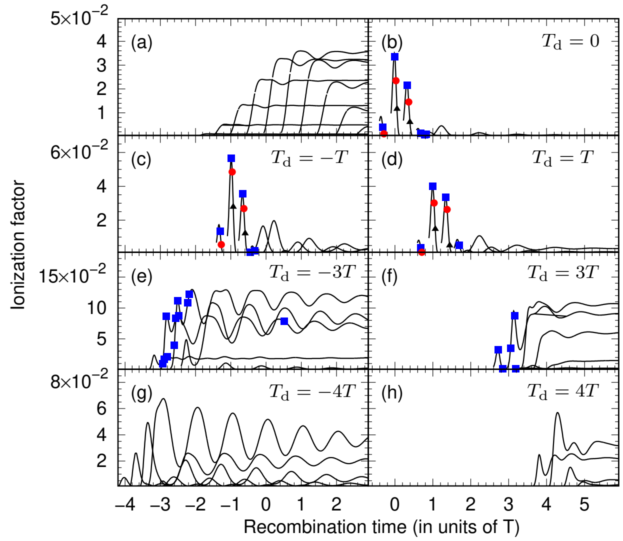

Figure 6. Dependence of the tunneling ionization factor (including the depletion factor), $|\mathcal{P}_j a_j^{(\rm tun)}|$ [cf. Eqs (23), (26)], on the recombination time, t_j, for seven different time delays between the two components of the bicircular pulse: (a) reference results for a single-color linearly polarized pulse with $I = 10^{14}$ W/cm^2, $\lambda = 1.6$ μm, and $N_1 = 4$; (b) $T_{\rm d} = 0$, (c) $T_{\rm d} = -T$, (d) $T_{\rm d} = T$, (e) $T_{\rm d} = -3T$, (f) $T_{\rm d} = 3T$, (g) $T_{\rm d} = -4T$, (h) $T_{\rm d} = 4T$. Symbols mark the ionization factors at the recombination times for $E = 2u_p$ (blue squares), $E = 3u_p$ (red circles), and $E = 4u_p$ (black triangles). Results in panels (b)-(h) are for a bicircular field (49) with $\lambda = 1.6$ μm, $I = 10^{14}$W/cm^2, $N_1 = 4$, $N_2 = 2$.

the recombination time, t_j, as a parameter. Depending on the time delay between the two components of the bicircular field, there are several branches of solutions of the transcendental Eq. (21a). We plot in Fig. 6 the dependence of the ionization factor on the recombination time, with the separate curves in Fig. 6 for a given time delay corresponding to the different branches of the solution of Eq. (21a). Changing the time delay changes the magnitude of the ionization factor dramatically [e.g., compare the results in Fig. 6(e) with those in the other panels]. Thus the time delay between the two components of the driving pulse can "optimize" the classical trajectories, thus enhancing (or otherwise controlling) ionization.

The constraint on the recombination time is given by Eq. (21b). Once Eq. (21a) is solved with respect to the ionization time t'_j, Eq. (21b) is the transcendental equation that must be solved for t_j. Real solutions of Eq. (21b) exist for some range of energies E. Thus the joint solution of Eqs. (21a) and (21b) gives the sets of times $\{t'_j, t_j\}$ that determine the closed classical trajectories. The marked points in Fig. 6 are the values of the ionization factor corresponding to the desired solutions of the system (21) for a given harmonic energy. For some time delays and energies E, there are no real solutions, such as, e.g., for the long time delays, $T_{\rm d} = \pm 4T$, in Fig. 6, whose curves thus have no marked points for the three energies $E = 2u_p$, $3u_p$, and $4u_p$ for which there are solutions for other time delays. For such long time delays, real solutions exist only for small energies, $E < 2u_p$ [see, e.g., Fig. 8(a)].

Trajectories with the shortest travel times are similar to the one shown in Fig. 2(c). Trajectories with long travel times have several turning points (cf. Fig 7). For *large negative* time delays, we find surprisingly long trajectories. These are initially driven by the 2ω-component of the pulse near the ionization time, and then brought back by the ω-component near the recombination time. We did not observe similarly long trajectories for *large positive* time delays (i.e., when the 2ω component of the driving field arrives later).

The physics underlying the presence of such long trajectories for negative time delays and their absence for positive delays is as follows: the momentum gained from the 2ω-field is less than half that gained in the ω-field. Thus, the ω-component of the field can overcome the electron's outgoing spiral motion in the circularly polarized 2ω-field, even at lower field strengths. The converse is not the case. Specifically, in the 2ω-field the electron moves along an outgoing spiral arc (see the left panel in the first row in Fig. 7). When the contribution of the ω-field to the electron momentum becomes comparable with that of the 2ω-field (see the middle panel of the first row in Fig. 7), it turns the trajectory around and brings it back along an incoming spiral trajectory, returning the electron to the origin after some time (see the right panel in the first row in Fig. 7).

The existence of closed classical trajectories with nonzero initial momentum in a circularly polarized field is not surprising and has been discussed in Ref. [132]. In a bicircular field, the 2ω-component gives the electron an initial "kick" (i.e., its initial momentum), following which the ω-component then returns the electron to the origin. The energy gained along such a long closed trajectory is of the order of $2u_p$ (or less). The plateau structures associated with these trajectories are shorter than those

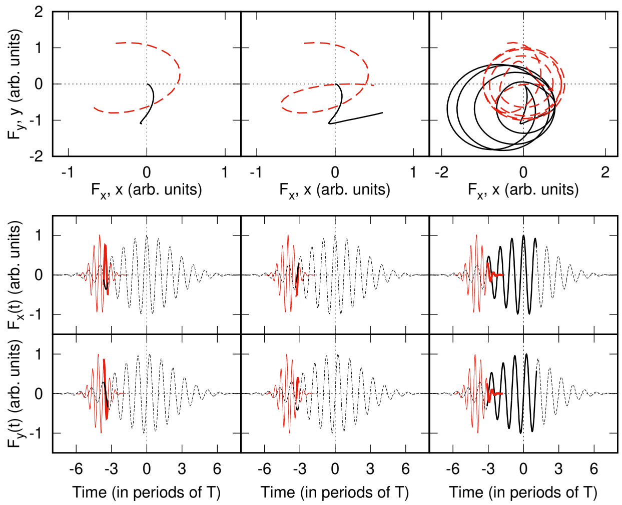

Figure 7. Illustrations of three stages in the formation of the long travel-time trajectories over three different time intervals. Left column: the "2ω-kick" stage; middle column: the"turn around" stage; right column: the "spiral-in" stage, driven by the ω-field. *Top row*: the x, y coordinates of the electron trajectories (solid black lines) and the $F_x(t), F_y(t)$ field trajectories (dashed red lines) over the time intervals discussed below. *Middle and Bottom rows*: $F_x(t)$ and $F_y(t)$ respectively for the 2ω (solid red lines) and ω (dashed black lines) field pulses. *The time intervals* for the stages in the top row are indicated by the thick parts of the field curves in the middle and bottom rows. The thin lines show the entire time evolution of the pulses. The calculations were done for the same laser parameters as in Fig. 6 with $T_{\rm d} = -4T$.

observed for the short travel time trajectories produced by bicircular fields having small two-color delays.

The spike-like behavior of the ionization factor observed for a time-delayed bicircular field [see Figs. 6(b)-(d)] contrasts with its rather flat behavior for the case of linear polarization [see Fig. 6(a)]. At some energies, the ionization factor may reach a maximum value, decreasing gradually with further increases in the return energy, thereby suppressing the contribution of the corresponding harmonic dipoles $\boldsymbol{d}_j$ (see Fig. 8) and resulting in a gradual decrease in the HHG yield. In contrast, for linear polarization, the ionization factor is almost flat for a wide range of return times, leading to a well-pronounced plateau. For large two-color time delays, the ionization factor behaves similarly to the case of linear polarization [see Figs. 6(e)-(h)] and hence the plateau structure is more pronounced.

D. The two-dipole model and time-delay control of HHG yields and polarizations

The adiabatic approximation results in Figs. 6 and 8 show that for moderate time delays between the bicircular pulses there are two contributing trajectories that determine the properties of the partial dipoles associated with the most important two ionization bursts [see Eq. (22)]. The HHG spectrum can thus be described as the emission by a system of *two* dipoles oscillating at frequency Ω. More specifically, these are two non-collinear dipoles having a mutual angle α and a phase difference Φ, as sketched in Fig. 9. This contrasts to the case of a long bicircular pulse, whose field has a trefoil shape that allows it to be described as *three* phase-locked dipoles having a relative angle of 120° between one another. Varying the time delay between the two components in a short bicircular pulse provides a means for controlling both the magnitudes of the two dipoles and the relative phase between them and hence a means for controlling both the HHG yields and the harmonic polarizations, as we show below.

According to Eq. (35), the magnitudes of the two dipoles are mainly determined by the ionization (including depletion effects), which is controlled by the time delay (see Fig. 6). The relative phase between two dipoles is given by the difference of the two classical actions for the electron moving along the two closed trajectories:

$$\begin{aligned} \Phi &= \Delta S + \Omega(t_1 - t_2), \\ \Delta S &= S(t_1, t_1') - S(t_2, t_2'), \end{aligned} \tag{50}$$

where $S(t, t')$ is given by Eq. (C3). The angle α is slightly sensitive to the time delay, but varies around the value of 120°.

Calculating the HHG yield and the degree of circular polarization for this two-dipole model $\boldsymbol{D}(\Omega) = \boldsymbol{d}_1 + \boldsymbol{d}_2 e^{-i\Phi}$ [using Eqs. (28) and (44)] leads to the expressions:

$$\rho(\Omega) = \frac{\Omega^4 d_1 d_2}{2c^3} \left[\delta + \cos\alpha\cos\Phi\right], \tag{51a}$$

$$\xi = -\frac{\sin\alpha\sin\Phi}{\delta + \cos\alpha\cos\Phi}, \tag{51b}$$

where $\delta = (d_1^2 + d_2^2)/(2d_1 d_2)$ and $\alpha \simeq 120°$. If the relative phase between the two dipoles is $\Phi = 2\pi n$ or $\Phi = \pi + 2\pi n$, then according to Eq. (51) linearly polarized light is emitted with intensity $\rho(\Omega) = \Omega^4 d_1 d_2/(2c^3)\left[\delta \pm \cos\alpha\right]$ (where the "+" sign corresponds to the first phase and "−" to the second one). Alternatively, if $\Phi = \pi/2 + \pi n$ then elliptically polarized light is emitted with $|\xi| = \sin\alpha/\delta$ and intensity $\rho(\Omega) = \Omega^4(d_1^2 + d_2^2)/(4c^3)$. Calculation of the maximum and minimum values of the polarization ξ with variation of the phase Φ gives $|\xi| = \sin\alpha/(\delta\sqrt{1 - \delta^{-2}\cos^2\alpha})$ with intensity $\rho(\Omega) = \Omega^4(d_1^2 + d_2^2)/(4c^3)\left[1 - \delta^{-2}\cos^2\alpha\right]$. Thus, by varying the phase Φ one can control the ellipticity over a wide range.

According to Eq. (50) applicable to our two-dipole model, the phase Φ is determined by the sum of two terms. One term is a linear function of the harmonic frequency Ω with coefficient $t_1 - t_2$. The other term is the difference ΔS, which depends on the time delay and can be changed by varying $T_{\rm d}$. For fixed laser parameters, the difference $t_1 - t_2$ is about one-third of the period T, so that the phase $\Phi \propto 2\pi(\Omega/3\omega)$ induces a

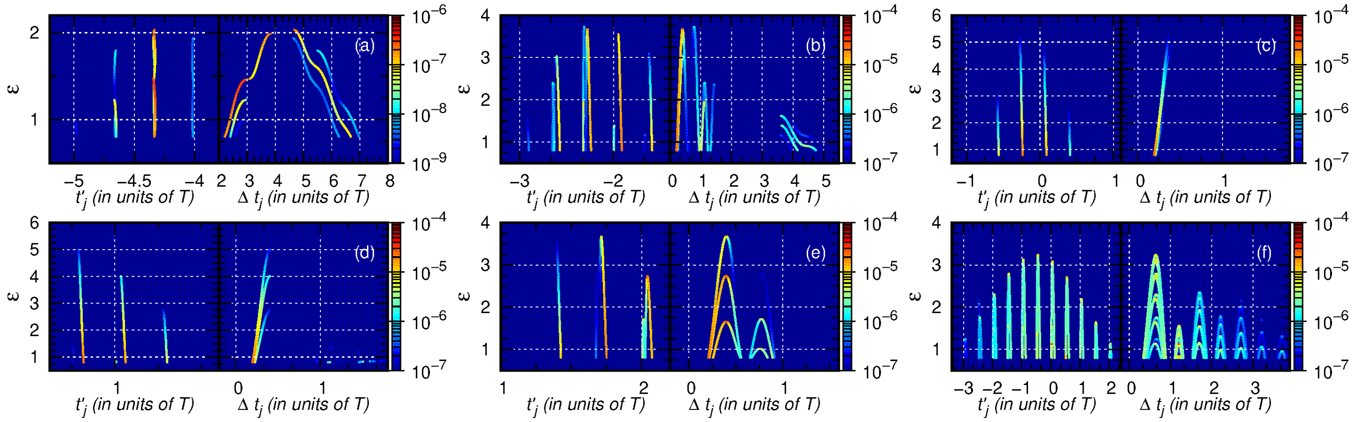

Figure 8. Dependence of the scaled return energy $\varepsilon = E/u_p$ [where $u_p = F^2/(4\omega^2)$] on the ionization time t'_j of the jth trajectory and the travel time Δt_j for the bicircular field (49) with $\lambda = 1.6\ \mu$m, $I = 10^{14}\mathrm{W/cm}^2$, $N_1 = 4$, $N_2 = 2$, and different two-color time delays: (a) $T_\mathrm{d} = -5T$; (b) $T_\mathrm{d} = -2T$; (c) $T_\mathrm{d} = 0$; (d) $T_\mathrm{d} = T$; (e) $T_\mathrm{d} = 2T$; (f) the case of linear polarization for $I = 2 \times 10^{14}$ W/cm^2. The color scale shows the relative contributions of the dipoles, $\propto |\boldsymbol{d}_j|$.

regular oscillation pattern in the HHG spectrum with a period 3ω (see Figs. 3 and 10). The maxima of these oscillations can be tuned to the positions of the forbidden harmonics by changing the time delay between the two incident pulses in the bicircular field [109]. Thus, for $\Delta S = (2n+1)\pi$ (where n is an integer), Eq. (51a) gives maxima for $\Omega = 3N\omega$, and, according to Eq. (51b), at these maxima $\xi = 0$.

We emphasize that our two-dipole analysis assumes a linear dependence of Φ on Ω and the equality $t_1 - t_2 = T/3$. This analysis is not applicable over the entire HHG spectrum. Hence, some deviations from the simple two-dipole model can be observed. However, by tuning the time delay between the two bicircular pulses, the locations of the maxima of the HHG spectrum oscillations at $\Omega = 3N\omega$, as well as the linear polarization of these "harmonics," can be produced over any finite range of values of the harmonics Ω.

Our two-dipole model also cannot in general describe the entire HHG spectrum, as the shape of the HHG spectrum in particular energy regions depends significantly on the number of contributing trajectories, which depends in turn on the two-color time delay. In Fig. 11 we present HHG spectra for different time delays over a much larger energy region than in Fig. 10. If there is only *one* contributing trajectory, then the HHG spectrum exhibits a smooth dependence on the scaled energy (see Fig. 11 for $T_\mathrm{d} = T$ and $T_\mathrm{d} = -T$ over the energy ranges $4 < E/u_p < 5$ and $4.5 < E/u_p < 5$, respectively). As discussed above, if there are *two* contributing trajectories, the HHG spectrum shows a regular large-scale oscillation. For small electron return energies, there are *several* contributing trajectories and their interference induces both large-scale and fine-scale oscillations.

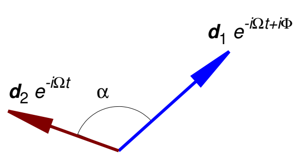

Figure 9. Sketch of the two-dipole model system.

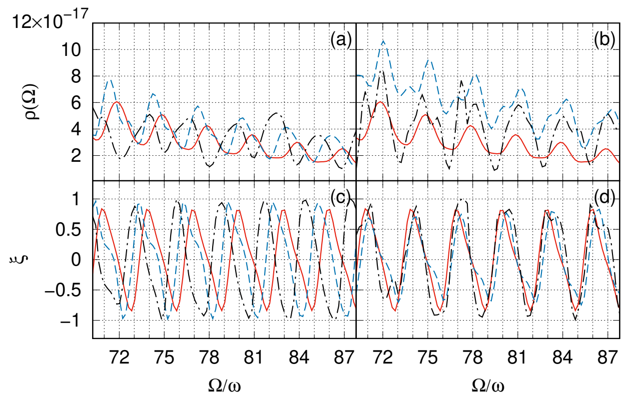

Figure 10. Illustration of the 3ω periodicity of both the HHG spectral density, $\rho(\Omega)$, (a, b) and the degree of circular polarization, ξ, (c, d) as functions of the harmonic number Ω/ω for five different time delays, T_d, and for the bicircular field parameters as in Fig. 6 (for which, $\omega = 0.0285$ a.u.). (a) and (c): Solid (red) lines (HHG yield is multiplied by four): $T_\mathrm{d} = 0$; dashed (blue) lines (HHG yield is multiplied by three): $T_\mathrm{d} = T$; dash-dot (black) lines: $T_\mathrm{d} = 2T$. (b) and (d): Solid (red) lines (HHG yield is multiplied by four): $T_\mathrm{d} = 0$; dashed (blue) lines (HHG yield is multiplied by three): $T_\mathrm{d} = -T$; dash-dot (black) lines: $T_\mathrm{d} = -2T$.

In general, few trajectories contribute at large harmonic energies and the few non-dominant trajectories only slightly perturb the smooth dependence associated with one dominant trajectory (see Fig. 11 for $T_\mathrm{d} = 2T$ for $2.7 < E/u_p < 3.7$) or the large-scale oscillations associated with two dominant trajectories (see Fig. 11 for $T_\mathrm{d} = 2T$ for $1.5 < E/u_p < 2.7$). As also shown in Fig. 11,

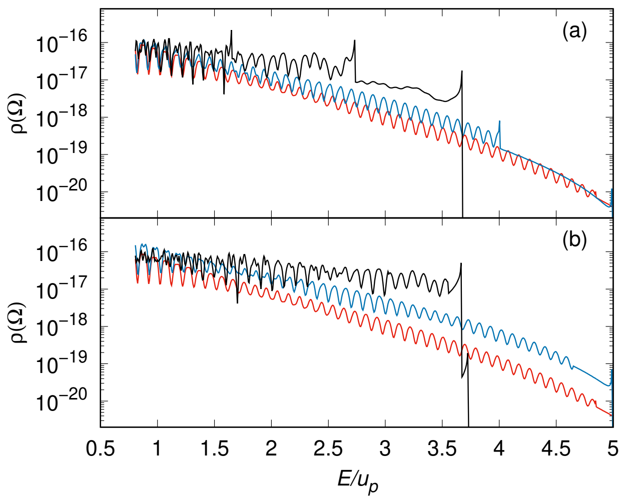

Figure 11. HHG spectral density, $\rho(\Omega)$, as a function of the electron's scaled return energy, E/u_p for five different time delays, T_d. Laser parameters are the same as in Fig. 10 and $u_p = F^2/(4\omega^2) = 0.88$ a.u. (a) Dashed (blue) line: $T_\mathrm{d} = T$; dash-dot (black) line; $T_\mathrm{d} = 2T$. (b) Dashed (blue) line: $T_\mathrm{d} = -T$; dash-dot (black) line: $T_\mathrm{d} = -2T$. In both panels, the solid (red) lines (with the HHG spectral density, $\rho(\Omega)$, multiplied by four): $T_\mathrm{d} = 0$.

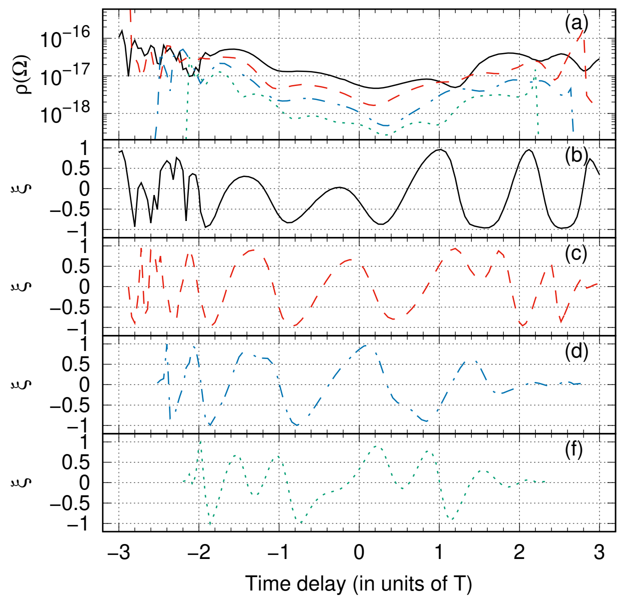

Figure 12. Dependence of the HHG spectral density, $\rho(\Omega)$, (a) and the circular polarization degree, ξ, (b)-(f) on the two-color time delay, T_d, for four harmonic energies, Ω. Solid lines: $\Omega = 2.26$ a.u.; dashed lines: $\Omega = 2.7$ a.u.; dot-dashed lines: $\Omega = 3.14$ a.u.; dotted lines: $\Omega = 3.57$ a.u. Results are for the same laser parameters as in Fig. 6.

increasing the time delay (from $\pm T$ to $\pm 2T$), one observes about an order of magnitude increase in the HHG yield in the high-energy part of the spectrum [109]. This enhancement originates from the favorable conditions for tunnel ionization at large time delays [see Fig. 6(e)]; however, it comes at the cost of a significant reduction in the HHG cutoff energy. For some energies the analytical HHG spectra show discontinuities or sharp peaks [see, e.g., the peaks in Fig. 11 (a) for $T_\mathrm{d} = 2T$ near the energies $E/u_p = 1.65$, 2.7 and 3.7]. These unphysical peculiarities are related to limitations of the analytic approach, which cannot be used for energies at which the product $\boldsymbol{K}_j \cdot \dot{\boldsymbol{K}}_j$ is close to zero [cf. Eqs. (24) and (35)]. These energies correspond to the bifurcation points (caustics) at which two trajectories coalesce, which requires a special treatment [120–122]. The largest of these energies gives an upper limit of energies for which the present analytic approach is applicable.

The most significant prediction of our two-dipole model analysis is that the time delay, T_d, between the two-color components of a short bicircular field provides a sensitive means of controlling the polarization properties as well as the yield of the generated harmonic light at a fixed harmonic energy, Ω. This HHG control is most effective if the time delay is of the order of a few periods, T, of the ω-field of the few-cycle bicircular driving pulses. These predictions are illustrated in Fig. 12, which shows the dependence of the harmonic yield and the degree of circular polarization on the time delay for four different harmonic energies. Fine-scale oscillations are observed in both the HHG yield and the degree of circular polarization for large negative time delays owing to the contributions of more than two dominant bursts in the harmonic dipoles (see Fig. 12 for $T_\mathrm{d} < -2T$). For small negative time delays and for positive time delays, the oscillation pattern is regular and results from the contributions of the two dominant dipoles. Most importantly, the results in Fig. 12 clearly show that variation of the two-color time delay over a single period T allows one to change the polarization of a given harmonic from left to right circular without changing the helicities of the two bicircular field components of the driving laser pulse.

V. SUMMARY AND OUTLOOK

In this paper we have used TDER theory, for a system with two bound states, to develop an analytic description of HHG driven by a laser field with an arbitrary waveform. The applicability of our approach requires the smallness of the imaginary part of the corresponding saddle-point ionization time, which obtains for the case of a laser field with a sufficiently low carrier frequency (or frequencies). In this description, the laser-induced dipole moment is a coherent sum of partial dipole moments, whose properties (direction, phase, and magnitude) are determined by the classical (real) times of ionization and recombination. These times determine the closed classical trajectories along which the ionized electron starts, with minimal kinetic energy, in the laser field [see Eq. (21a)] and returns back with the kinetic energy corresponding to harmonic emission with frequency Ω [see Eq. (21b)]. The partial dipole moment for a system with an active s-electron can be written as a product of three factors [see Eq. (22)]: the ionization factor, the propagation factor, and the exact photorecombination amplitude. This result theoretically justifies the quasiclassical factorization of the HHG yield in terms of an EWP and the exact TDER photorecombination cross section (for the case of an active electron in an s-state) for a laser field having an arbitrary waveform.

The results for our TDER model system were extended to the case of a neutral atom, in which the Coulomb field effects are crucial, by making two modifications: (i) Using closed form analytical TDER expressions for the laser-induced dipole moment in which we introduce the Coulomb corrections in Eq. (34) for the ionization factor; and (ii) Replacing the TDER photorecombination amplitude by its atomic counterpart. Our precise numerical solutions of the 3D TDSE for a low-frequency bicircular field were found to be in excellent agreement with the analytical results for the H atom (see Figs. 3-5), thus confirming the accuracy of our analytical description. This analytical model provides one with reliable tools to analyze HHG in intense MIR driving fields composed of multiple phase-locked colors with complex polarization states.

Our analytic results for the yields and the polarizations of the generated harmonics were obtained for the cases of both long and short time delays, T_d, between the two components of the bicircular pulses. In both cases we demonstrated the crucial role of ionization, which changes drastically the shapes of HHG spectra and the polarization properties of the emitted harmonics. In the case of long time delays, the ionization factor reduces the number of partial dipoles (trajectories) that contribute to harmonic emission at a particular frequency, thus smoothing the sharp peaks at $\Omega = (3N \pm 1)\omega$ dictated by dipole selection rules. Moreover, ionization also affects the polarization properties of the emitted harmonics, leading to deviations from the simple predictions based on the dipole selection rules.

In the case of short time delays, we demonstrated that the time delay controls the ionization and recombination times, thus allowing one to control HHG yields and, most important, the polarizations of the emitted harmonics. Enhancement of HHG yields can be effected by controlling the ionization factors in the contributions of different partial dipoles associated with successive ionization bursts. Varying the time delay may increase the HHG intensity by creating favorable conditions for ionization (conditioned on the return of the launched trajectory).

For the case of a few-cycle bicircular laser field, both the shape of the HHG spectrum and the polarization properties of the emitted harmonics can be modeled by assuming the major contributions stem from two dominant dipoles with different orientations and magnitudes. This two-dipole model accurately predicts the oscillation patterns in the HHG spectrum and the dependence of the degree of circular polarization of the harmonics on the harmonic energy. Efficient control of the HHG process is achieved by varying the classical actions of the two dominant trajectories, which is accomplished by changing the time delay between the two-color components of a short bicircular pulse.

Finally, we have focused in this paper on the simplest case in which the active electron is in an initial s-state. The case of an initial p-state requires a separate analysis owing to the facts that there are three contributing magnetic sublevels and that the recombination amplitude to these states or their linear combinations has a tensor form [cf. Eq. (12) in Ref. [84]]. These features may lead to a parametrization of the induced dipole moment that prevents one from factorizing the HHG yield in terms of an EWP and the photorecombination cross section for the case of an arbitrary driving laser pulse waveform (cf. Refs. [84, 85]). On the other hand, the study of HHG from p-states for the case of a general driving laser pulse waveform may suggest improvements of current schemes for HHG-spectroscopy.

ACKNOWLEDGMENTS

This work was supported in part by the Ministry of Science and Higher Education of the Russian Federation through Grant No. 3.1659.2017/4.6, by the Russian Science Foundation through Grant No. 18-12-00476 (numerical calculations and model development), and by the U.S. National Science Foundation through Grant No. PHY-1505492 (A. F. S.). M. Yu. I. acknowledges the support of a DFG QUTIF grant.

Appendix A: Justification of the boundary condition in Eq. (1) for strong laser field processes

The boundary condition for the stationary state wave function $\Psi_\epsilon(\boldsymbol{r})$ of a weakly-bound electron in static magnetic and electric fields was formulated in Refs. [75, 76]:

$$\begin{aligned} &\int \Psi_\epsilon(\boldsymbol{r}) Y^*_{l\,m}(\Omega) d\Omega \\ &= f_0^{(l,m)} \left[\left(r^{-l-1} + \cdots \right) + \mathcal{B}_l(\epsilon) \left(r^l + \cdots \right) \right], \qquad \text{(A1)} \\ &(2l-1)!!(2l+1)!!\mathcal{B}_l(\epsilon) = k^{2l+1} \cot \delta_l(k), \quad k = \sqrt{2\epsilon}. \end{aligned}$$

Equation (A1) is based on the well-known expansion of a scattering wave function for a low-energy electron in a short-range potential (see Sec. 132 in Ref. [43]). Its range of applicability is given by the inequality $ka \ll 1$, where a is the radius of the short-range potential. In calculating the energy of a weakly-bound electron in two stationary potentials with predominantly different ranges (i.e., short- and long-range potentials) [75, 76], it is assumed that the energy is located near the continuum threshold and, to simplify the dependence of $\mathcal{B}_l(\epsilon)$ on energy, a two-term series expansion in energy is used for $\mathcal{B}_l(\epsilon)$. These two terms are parameterized in terms of the scattering length and the effective range [43].

At first sight, the boundary condition (A1) cannot be employed for fast electrons. However, in scattering of fast electrons the major contribution is given by small distances ($kr \ll 1$), i.e., the electron effectively "feels" the potential at smaller distances than the actual radius a of the short-range potential. Based on this physical assumption, a model may be proposed for which an atomic potential has an effective radius $\tilde{a}$, for which the condition $k\tilde{a} \ll 1$ is fulfilled. Thus the expansion (A1) can be formally applied, although the scattering phase cannot be expanded in a series in k^2. This model is known as the hard-sphere model formulated in terms of a pseudopotential [133] (see also Ref. [134]).

The boundary condition (A1) should be modified for the case of the long-range, periodic-in-time electron-laser interaction [73, 74]. Indeed, in accord with the theory of quasistationary quasienergy states [77, 116], the wave function for a complex quasienergy ϵ has the form,

$$\Psi(\boldsymbol{r},t) = e^{-i\epsilon t}\Phi_\epsilon(\boldsymbol{r},t), \quad \Phi_\epsilon(\boldsymbol{r},t+\mathcal{T}) = \Phi_\epsilon(\boldsymbol{r},t), \tag{A2}$$

where $\mathcal{T}$ is the period of the electron-laser interaction, and the periodic function $\Phi_\epsilon(\boldsymbol{r},t)$ is the solution of the equation,

$$\left[H_0(\boldsymbol{r}) + V(\boldsymbol{r},t) - i\frac{\partial}{\partial t}\right]\Phi_\epsilon(\boldsymbol{r},t) = \epsilon\Phi_\epsilon(\boldsymbol{r},t). \tag{A3}$$

In Eq. (A3), $H_0(\boldsymbol{r}) = -\nabla^2/2 + U(r)$ is the unperturbed Hamiltonian, where $U(r)$ is the atomic potential, and $V(\boldsymbol{r},t) = V(\boldsymbol{r},t+\mathcal{T})$ is the periodic-in-time potential of the electron-laser interaction,

$$V(\boldsymbol{r},t) = \boldsymbol{r}\cdot\boldsymbol{F}(t), \tag{A4}$$

where we have used the length-gauge dipole approximation for $V(\boldsymbol{r},t)$ in which $\boldsymbol{F}(t)$ is the electric component of the laser field.

As we have discussed in Ref. [74], the two potentials, $U(r)$ and $V(\boldsymbol{r},t)$, are significant in two very different radial ranges: the potential $U(r)$ is important for $r \lesssim \tilde{a}$, whereas the potential $V(\boldsymbol{r},t)$ is significant for $r \gg \tilde{a}$. Thus, for $r \sim \tilde{a}$ the electron can be considered to be essentially free. In this region, Eq. (A3) can be analyzed by omitting the potentials $U(r)$ and $V(\boldsymbol{r},t)$. Hence, for the l-wave channel, the solution of Eq. (A3) can be sought in a form similar to that in Eq. (A1). Owing to the time derivative in Eq. (A3), the solution for energy ϵ can be "replicated" by that for "energy" $\mathcal{E}_n = \epsilon + n\omega_\tau$ by subsequent multiplication by the exponential $e^{-in\omega_\tau t}$, where $\omega_\tau = 2\pi/\mathcal{T}$. The desired result for the periodic solution for $r \sim \tilde{a}$ thus has the form,

$$\begin{aligned}&\int \Phi_\epsilon(\boldsymbol{r},t)Y^*_{lm}(\Omega)d\Omega\\ &= \sum_n f_n^{(l,m)}\left[\left(r^{-l-1}+\cdots\right)\right.\\ &\left.+\mathcal{B}_l(\mathcal{E}_n)\left(r^l+\cdots\right)\right]e^{-in\omega_\tau t}, \quad \mathcal{E}_n = \epsilon + n\omega_\tau,\end{aligned} \tag{A5}$$

where $f_n^{(l,m)}$ are Fourier coefficients of a periodic function $f^{(l,m)}(t) = \sum_n f_n^{(l,m)} e^{-in\omega_\tau t}$. Since the sum in Eq. (A5) is over all n, it assumes that $\mathcal{E}_n$ may be large. However, the convergence of the Fourier series to the function $f^{(l,m)}(t)$ dictates an exponential decrease of the coefficients $f_n^{(l,m)}$ for large $|n|$ [74]. Hence, there is some effective upper limit ($\mathcal{E}_\mathrm{e}$) for the energies $\mathcal{E}_n$ that contribute, which allows one to estimate $\tilde{a}$, i.e., $\tilde{a} \sim 1/\sqrt{2\mathcal{E}_\mathrm{e}}$, thus ensuring the validity of the condition $\sqrt{2\mathcal{E}_n}\tilde{a} \lesssim 1$. Consequently, in Eq. (A5) one may use the parametrization of $\mathcal{B}_l(\mathcal{E}_n)$ in terms of the exact scattering phases $\delta_l(k)$ (without expansion in k) [cf. Eq. (A1)] up to energies $\sim \mathcal{E}_\mathrm{e}$.

Appendix B: Derivation of $\Delta\epsilon$ in Eq. (8) and the harmonic amplitude (11) in the TDER model

In the strong-field, low-frequency regime (in which the carrier frequency of the laser pulse is much smaller than the ionization potential I_p of the atom), $\Delta(t,t') \gg 1$ and integrals containing $\mathcal{G}_\epsilon(t,t')$ are exponentially small [see Eqs. (5d), (5e), (6), and (7)]. In the adiabatic approach one retains terms that are of first order in these exponentially small quantities and ignores those of higher order [81, 90, 91]. Thus the equation for the complex quasienergy, ϵ, of the initial s-state in the two-component field can be obtained from Eq. (6a) for $n = 0$ by substituting $f^{(0,0)}(t) = f_0^{(0,0)}$ and coefficients $f_n^{(1,m)}$ from Eq. (7b) for the function $f^{(1,m)}(t)$. We also neglect the contribution of the laser field to the function $\mathcal{G}_\epsilon(t,t')$ in the second term on the right-hand side of Eq. (6a) by making the substitution $\mathcal{G}_\epsilon(t,t') \to e^{i\epsilon(t-t')}/[\sqrt{2\pi i}(t-t')^{3/2}]$. Thus, in the adiabatic approximation, the equation for the complex quasienergy takes the form:

$$\begin{aligned}&\mathcal{B}_0(\epsilon) - i\varkappa_0\\ &= \frac{1}{\mathcal{T}}\int_{-\mathcal{T}/2}^{\mathcal{T}/2}\int_{-\infty}^{t}\frac{\left[e^{i\widetilde{\Delta}(t,t')}-1\right]e^{i\epsilon(t-t')}}{\sqrt{2\pi i}(t-t')^{3/2}}dt'dt\\ &-\sum_m \frac{i\sqrt{3}}{\mathcal{T}f_0^{(0,0)}}\int\limits_{-\mathcal{T}/2}^{\mathcal{T}/2}\int\limits_{-\infty}^{t}\frac{e^{i\epsilon(t-t')}f^{(1,m)}(t')}{\sqrt{2\pi i}(t-t')^{3/2}}\widetilde{K}'_m dt'dt,\end{aligned} \tag{B1}$$

where $\widetilde{\Delta}(t,t')$ and $\widetilde{K}'_m$ are given by Eqs. (5e) and (3), respectively, with the substitution $\boldsymbol{A}(t) \to \widetilde{\boldsymbol{A}}(t)$.

Assuming that the harmonic field amplitude, F_Ω, is small (see Sec. II B), we write ϵ as the sum $\epsilon = \epsilon_0 + \Delta\epsilon$, where ϵ_0 is the complex quasienergy in the strong periodic field alone and $\Delta\epsilon$ gives a correction linear in F_Ω. Specifically, ϵ_0 obeys Eq. (B1) for $F_\Omega = 0$, in which the strong field is given by the vector potential $\boldsymbol{A}_\tau(t)$, and $\Delta\epsilon \propto F_\Omega$.

In order to obtain an explicit expression for $\Delta\epsilon$, we expand the left- and right-hand sides of Eq. (B1) in a series in F_Ω up to first order. As a result, we obtain the following expression for $\Delta\epsilon$:

$$
\begin{aligned}
\Delta\epsilon =& -\frac{1}{\mathcal{N}\mathcal{T}}\sqrt{\frac{i}{2\pi}}\int_{-\mathcal{T}/2}^{\mathcal{T}/2}\int_{-\infty}^{t}\frac{e^{i\Delta_\tau(t,t')+i\epsilon_0(t-t')}}{(t-t')^{3/2}}\left[\boldsymbol{F}_\Omega\cdot\boldsymbol{G}(\Omega)+\boldsymbol{F}_\Omega^{*}\cdot\boldsymbol{G}(-\Omega)\right]dt'dt \\
& -\frac{\sqrt{3}}{\mathcal{N}f_0^{(0,0)}}\sum_m\left[a(\Omega)(\boldsymbol{F}_\Omega)_m f_{-N}^{(1,m)}+a(-\Omega)(\boldsymbol{F}_\Omega^{*})_m f_{N}^{(1,m)}\right], && \text{(B2)}\\
a(\Omega) =& \frac{1}{2\Omega\sqrt{2\pi i}}\int_0^\infty\frac{e^{i\epsilon_0\tau}}{\tau^{3/2}}\left(1+\frac{e^{-i\Omega\tau}-1}{i\Omega\tau}\right)d\tau=\frac{i}{2\Omega}\left\{\sqrt{2\epsilon_0}+\frac{(2\epsilon_0-2\Omega)^{3/2}}{3\Omega}-\frac{(2\epsilon_0)^{3/2}}{3\Omega}\right\}, && \text{(B3)}\\
\mathcal{N} =& \frac{\partial\mathcal{B}(\epsilon_0)}{\partial\epsilon_0}-\frac{1}{\sqrt{-2\epsilon_0}}-\sqrt{\frac{i}{2\pi}}\frac{1}{\mathcal{T}}\int\limits_{-\mathcal{T}/2}^{\mathcal{T}/2}\int_{-\infty}^{t}\frac{\left[e^{i\Delta_\tau(t,t')}-1\right]e^{i\epsilon_0(t-t')}dt'dt}{(t-t')^{1/2}} \\
& -\sum_m\frac{\sqrt{3}}{\mathcal{T}}\int_{-\mathcal{T}/2}^{\mathcal{T}/2}\int_{-\infty}^{t}\frac{e^{i\epsilon_0(t-t')}f^{(1,m)}(t')}{\sqrt{2\pi i}(t-t')^{1/2}}K'_m dt'dt, && \text{(B4)}\\
\boldsymbol{G}(\Omega;t,t')\equiv\boldsymbol{G}(\Omega) =& \frac{1}{2i\Omega}\int_{t'}^{t}\boldsymbol{A}_\tau(\xi)e^{-i\Omega\xi}d\xi-\frac{1}{t-t'}\int_{t'}^{t}\boldsymbol{A}_\tau(\xi)d\xi\frac{e^{-i\Omega t}-e^{-i\Omega t'}}{2\Omega^2}, && \text{(B5)}
\end{aligned}
$$

where $\Delta_\tau(t,t')=\widetilde{\Delta}(t,t')|_{F_\Omega=0}$. Owing to the accuracy of the adiabatic approximation for long wavelength laser fields, one may replace the exact complex quasienergy in the field $\boldsymbol{A}_\tau(t)$ by its unperturbed value ($\epsilon_0\to-I_p$) in the integrals (B2)-(B4) [70]. Moreover, without loss of accuracy, Eq. (B4) can be evaluated for the field-free case, for which the last two integrals equal zero:

$$\mathcal{N}\approx r_0-\kappa^{-1}=-2C_\kappa^{-2}\kappa^{-1}. \qquad \text{(B6)}$$

To obtain Eq. (B6), we have replaced $\mathcal{B}(\epsilon_0)$ in Eq. (B4) by the effective range expansion $\mathcal{B}(\epsilon_0)\approx a_0^{-1}+r_0\epsilon_0$, where a_0 is the scattering length and r_0 is the effective range [43]. Note that C_κ in Eq. (B6) is the dimensionless asymptotic coefficient that determines the behavior of the field-free bound s-state at large distances:

$$\psi_0(\boldsymbol{r})\approx\sqrt{\kappa}C_\kappa\frac{e^{-\kappa r}}{r}Y_{00}(\hat{\boldsymbol{r}}),\quad \kappa=\sqrt{2I_p}. \qquad \text{(B7)}$$

Substituting the explicit form of the coefficients $f_N^{(1,m)}$ from Eq. (7b) into Eq. (B2) and noting that $(\boldsymbol{a}\cdot\boldsymbol{b})=\sum_{m=-1}^{1}(-1)^m a_m b_{-m}$, we obtain $\Delta\epsilon$ in the form:

$$
\begin{aligned}
\Delta\epsilon =& -\frac{1}{\mathcal{N}\mathcal{T}}\sqrt{\frac{i}{2\pi}}\int_{-\mathcal{T}/2}^{\mathcal{T}/2}\int_{-\infty}^{t}\frac{e^{i\Delta_\tau(t,t')-iI_p(t-t')}}{(t-t')^{3/2}} \\
& \times\left[\boldsymbol{F}_\Omega\cdot\boldsymbol{G}(\Omega)+\boldsymbol{F}_\Omega^{*}\cdot\boldsymbol{G}(-\Omega)+\frac{e^{-i\Omega t}a(\Omega)\boldsymbol{F}_\Omega\cdot\boldsymbol{K}_\tau(t,t')}{\mathcal{B}_1(-I_p-\Omega)-i\varkappa_{-N}^3/3}+\frac{e^{i\Omega t}a(-\Omega)\boldsymbol{F}_\Omega^{*}\cdot\boldsymbol{K}_\tau(t,t')}{\mathcal{B}_1(-I_p+\Omega)-i\varkappa_{N}^3/3}\right]dt'dt, \qquad \text{(B8)}
\end{aligned}
$$

where $\varkappa_{\pm N}=\sqrt{2(-I_p\pm\Omega)}$, $\Omega=N\omega_\tau$, and $\boldsymbol{K}_\tau(t,t')$ is given by Eq. (5e) with the substitution $\boldsymbol{A}(t)\to\boldsymbol{A}_\tau(t)$.

Doing the integrals in Eq. (B5) by parts, we transform (B5) to the following more appropriate form for further analysis:

$$
\begin{aligned}
\boldsymbol{G}(\Omega) =& \frac{e^{-i\Omega t}}{2\Omega^2}\boldsymbol{K}_\tau(t,t')-\frac{e^{-i\Omega t'}}{2\Omega^2}\boldsymbol{K}'_\tau(t,t') \\
& +\frac{1}{2\Omega^2}\int_{t'}^{t}\boldsymbol{F}_\tau(\xi)e^{-i\Omega\xi}d\xi,\quad \boldsymbol{F}_\tau(t)=-\frac{\partial\boldsymbol{A}_\tau(t)}{\partial t}, \qquad \text{(B9)}
\end{aligned}
$$

where $\boldsymbol{K}'_\tau(t,t')$ is given by Eq. (3) with the substitution $\boldsymbol{A}(t)\to\boldsymbol{A}_\tau(t)$. Taking into account Eq. (B9), substituting (B8) into Eq. (8), and then taking the limit (9) for fixed Ω, we obtain the dipole moment $\boldsymbol{D}(\Omega)$ in the form (11).

Appendix C: Analytic evaluation of the dipole moment (12) in the adiabatic limit

Before estimating the dipole moment (12), we estimate the integral in Eq. (13) using the saddle point method. The saddle points (t'_ν) are given by the equation:

$$\boldsymbol{K}'^2(t,t'_\nu)=-2I_p, \qquad \text{(C1)}$$

where $t'_\nu \equiv t'_\nu(t)$ is the ν-th *complex* root of Eq. (C1). We consider only those roots, t'_ν, that have positive imaginary parts, since the adiabatic transition to the continuum state starts from a bound state with negative energy $-I_p$ [43]. After saddle-point integration over t', $\boldsymbol{D}_1(t)$ takes the form:

$$\boldsymbol{D}_1(t) \approx -i\mathcal{C}\sum_\nu \frac{e^{iS(t,t'_\nu)}\boldsymbol{K}(t,t'_\nu)}{(t-t'_\nu)^{3/2}\sqrt{\alpha_\nu(t)}}g(\Omega), \tag{C2}$$

where

$$S(t,t') = -\frac{1}{2}\int_{t'}^{t}\left[\boldsymbol{A}(\xi) - \frac{1}{t-t'}\int_{t'}^{t}\boldsymbol{A}(\xi')d\xi'\right]^2 d\xi$$
$$-I_p(t-t'), \tag{C3}$$

$$\alpha_\nu(t) = \left.\frac{\partial^2 S(t,t')}{\partial t'^2}\right|_{t'=t'_\nu(t)} = \boldsymbol{K}'(t,t')\cdot\left.\frac{\partial \boldsymbol{K}'(t,t')}{\partial t'}\right|_{t'=t'_\nu(t)}$$
$$= -\left[\boldsymbol{F}(t'_\nu)\cdot\boldsymbol{K}'(t,t'_\nu) + \frac{2I_p}{t-t'_\nu}\right]. \tag{C4}$$

Substituting Eq. (C2) into Eq. (12), we obtain:

$$\boldsymbol{D}_1(\Omega) = -i\mathcal{C}\sum_\nu \int_{-\infty}^{\infty}\frac{e^{i\mathcal{S}_\nu(t)}\boldsymbol{K}(t,t'_\nu)}{(t-t'_\nu)^{3/2}\sqrt{\alpha_\nu(t)}}g(\Omega)dt, \tag{C5}$$

where

$$\mathcal{S}_\nu(t) = S(t,t'_\nu) + \Omega t. \tag{C6}$$

Since the contributions of the roots $t'_\nu(t)$ in the sum over ν in Eq. (C5) are determined by their imaginary parts, the roots with the smallest imaginary parts give the major contributions. Thus, we represent t'_ν as a sum of its real and imaginary parts: $t'_\nu = \overline{t'}_\nu + i\Delta t'_\nu$, where $\overline{t'}_\nu$ and $\Delta t'_\nu$ are real and $0 < \omega\Delta t'_\nu \ll 1$ (where ω is the carrier frequency of the laser pulse). Substituting this form for t'_ν in the left hand side of Eq. (C1) and expanding it in powers of $i\Delta t'_\nu$ up to second order, we obtain:

$$\boldsymbol{K}'^2(t,\overline{t'}_\nu) + i2\Delta t'_\nu \boldsymbol{K}'(t,\overline{t'}_\nu)\cdot\dot{\boldsymbol{K}}'(t,\overline{t'}_\nu)$$
$$-(\Delta t'_\nu)^2\left[\dot{\boldsymbol{K}}'^2(t,\overline{t'}_\nu) + \boldsymbol{K}'(t,\overline{t'}_\nu)\cdot\ddot{\boldsymbol{K}}'(t,\overline{t'}_\nu)\right]$$
$$= -\kappa^2, \tag{C7}$$

where $\dot{\boldsymbol{K}}'(t,\overline{t'}_\nu) = \partial\boldsymbol{K}'(t,t')/\partial t'\big|_{t'=\overline{t'}_\nu}$, and $\ddot{\boldsymbol{K}}'(t,\overline{t'}_\nu) = \partial^2\boldsymbol{K}'(t,t')/\partial t'^2\big|_{t'=\overline{t'}_\nu}$. Separating real and imaginary parts in Eq. (C7), we obtain two equations:

$$\boldsymbol{K}'(t,\overline{t'}_\nu)\cdot\dot{\boldsymbol{K}}'(t,\overline{t'}_\nu) = \left.\frac{\partial^2 S(t,t')}{\partial t'^2}\right|_{t'=\overline{t'}_\nu} = 0, \tag{C8a}$$

$$(\Delta t'_\nu)^2\mathcal{F}(t,\overline{t'}_\nu)^2 = \varkappa(t,\overline{t'}_\nu)^2, \tag{C8b}$$

where

$$\mathcal{F}(t,\overline{t'}_\nu) = \sqrt{\dot{\boldsymbol{K}}'^2(t,\overline{t'}_\nu) + \boldsymbol{K}'(t,\overline{t'}_\nu)\cdot\ddot{\boldsymbol{K}}'(t,\overline{t'}_\nu)}, \tag{C9}$$

$$\varkappa(t,\overline{t'}_\nu) = \sqrt{\kappa^2 + \boldsymbol{K}'^2(t,\overline{t'}_\nu)}. \tag{C10}$$

Equation (C8a) shows explicitly that the electron leaves the atom at the moment $\overline{t'}_\nu$, which ensures minimal kinetic energy at this moment. [Note that Eq. (C8a) for the case of linear polarization of the laser field reduces to $\boldsymbol{K}'(t,\overline{t'}_\nu) = 0$.] Equation (C8b) determines the "under-barrier" part of the tunneling time:

$$\Delta t'_\nu = \frac{\varkappa(t,\overline{t'}_\nu)}{\mathcal{F}(t,\overline{t'}_\nu)}. \tag{C11}$$

A simplification of $\mathcal{F}(t,\overline{t'}_\nu)$ in Eq. (C9) is achieved using Eq. (C8a) and the relations,

$$\dot{\boldsymbol{K}}'(t,\overline{t'}_\nu) = -\boldsymbol{F}(\overline{t'}_\nu) + \frac{\boldsymbol{K}'(t,\overline{t'}_\nu)}{t-t'_\nu},$$

$$\ddot{\boldsymbol{K}}'(t,\overline{t'}_\nu) = -\dot{\boldsymbol{F}}(\overline{t'}_\nu) - \frac{\boldsymbol{F}(\overline{t'}_\nu)}{t-t'_\nu} + \frac{2\boldsymbol{K}'(t,\overline{t'}_\nu)}{[t-t'_\nu]^2},$$

which lead to the following expression for $\mathcal{F}(t,\overline{t'}_\nu)$:

$$\mathcal{F}(t,\overline{t'}_\nu) = \sqrt{\boldsymbol{F}^2(\overline{t'}_\nu) - \boldsymbol{K}'(t,\overline{t'}_\nu)\cdot\dot{\boldsymbol{F}}(\overline{t'}_\nu)}, \tag{C12}$$

$$\dot{\boldsymbol{F}}(t) = \frac{\partial\boldsymbol{F}(t)}{\partial t}. \tag{C13}$$

We emphasize that the expression under the square root in Eq. (C12) is positive, because it is given by the second derivative of $\boldsymbol{K}'^2(t,t')$ in t', which is positive at the minimum of $\boldsymbol{K}'^2(t,t')$:

$$\frac{1}{2}\left.\frac{\partial^2\boldsymbol{K}'^2(t,t')}{\partial t'^2}\right|_{t'=\overline{t'_\nu}} = \dot{\boldsymbol{K}}'^2(t,\overline{t'}_\nu)$$
$$+\boldsymbol{K}'(t,\overline{t'}_\nu)\cdot\ddot{\boldsymbol{K}}'(t,\overline{t'}_\nu) > 0.$$

[Note that $\boldsymbol{K}'(t,\overline{t'}_\nu) = 0$ for the case of linear polarization and Eq. (C11) in this case reduces to the well-known result $\Delta t'_\nu = \kappa/|\boldsymbol{F}(\overline{t'}_\nu)|$.]

For small $\Delta t'_\nu$ ($\omega\Delta t'_\nu \ll 1$), we can calculate $\alpha_\nu(t)$ (C4) and the action $S(t,t')$ (C3) by expanding them in series up to the first and third order respectively in $\Delta t'_\nu$:

$$\alpha_\nu(t) \approx i\Delta t'_\nu\,\mathcal{F}^2(t,\overline{t'}_\nu), \tag{C14}$$

$$S(t,t'_\nu) \approx S(t,\overline{t'}_\nu) + \frac{i}{3}\frac{\varkappa^3(t,\overline{t'}_\nu)}{\mathcal{F}(t,\overline{t'}_\nu)}. \tag{C15}$$

Taking into account Eqs. (C11), (C14), and (C15), we obtain $\boldsymbol{D}_1(t)$ in Eq. (C2) in the form:

$$\boldsymbol{D}_1(t) = -\sqrt{i}\mathcal{C}\sum_\nu \frac{e^{-\frac{\varkappa^3(t,\overline{t'}_\nu)}{3\mathcal{F}(t,\overline{t'}_\nu)}}}{\sqrt{\varkappa(t,\overline{t'}_\nu)\mathcal{F}(t,\overline{t'}_\nu)}}$$
$$\times\frac{e^{iS(t,\overline{t'}_\nu)}\boldsymbol{K}(t,\overline{t'}_\nu)}{(t-\overline{t'_\nu})^{3/2}}g(\Omega). \tag{C16}$$

The dipole moment (C16) involves two rapidly varying exponents: one (the "tunneling exponent") is associated with tunneling, while the second (the "propagation exponent") is governed by the classical (*real-valued*) action for an electron moving in the laser field along a closed classical trajectory from the moment $\overline{t'}_\nu$ until the time t.

In the tunneling regime (in which $\omega\kappa/F \ll 1$, where F and ω are the laser field strength and frequency), the "propagation exponent" changes much faster than the "tunneling exponent" [by a factor $(\omega\kappa/F)^{-3}$]. Thus, to estimate the Fourier-component of $\boldsymbol{D}_1(t)$, we can treat the tunneling exponent as a "smooth" function. As a result, the position of the stationary phase of the integral (12), where $\boldsymbol{D}_1(t)$ is given by Eq. (C16), can be found from the equation:

$$\frac{\boldsymbol{K}^2(t,\overline{t'}_\nu)}{2} - \left(\frac{\boldsymbol{K}'^2(t,\overline{t'}_\nu)}{2} + I_p\right)\frac{d\overline{t'}_\nu}{dt} = E, \tag{C17}$$

where $E = \Omega - I_p$. Differentiating Eq. (C8a) with respect to t, we obtain $\dfrac{d\overline{t'}_\nu}{dt}$ in the form:

$$\begin{aligned}\frac{d\overline{t'}_\nu}{dt} = \frac{1}{(t-\overline{t'}_\nu)\mathcal{F}(t,\overline{t'}_\nu)^2}\Bigg\{&2\frac{\boldsymbol{K}(t,\overline{t'}_\nu)\cdot\boldsymbol{K}'(t,\overline{t'}_\nu)}{t-\overline{t'}_\nu} \\ &-\boldsymbol{F}(\overline{t'}_\nu)\cdot[\boldsymbol{K}(t,\overline{t'}_\nu) - \boldsymbol{K}'(t,\overline{t'}_\nu)]\Bigg\}.\end{aligned} \tag{C18}$$

Thus the equation for the stationary phase point is:

$$\frac{\boldsymbol{K}(t,\overline{t'}_\nu)^2}{2} = E + \Delta E_\nu(t), \tag{C19}$$

where

$$\Delta E_\nu(t) = -\frac{\boldsymbol{K}'(t,\overline{t'}_\nu)^2 + \kappa^2}{2(t-\overline{t'}_\nu)}\frac{d\overline{t'}_\nu}{dt}, \tag{C20}$$

which we interpret as a quantum correction to the energy gained by the electron in the laser field (cf. Ref. [34]).

In order to simplify the notations further, we introduce here a single index, j, to enumerate the joint solutions of Eqs. (C8a) and (C19), which we present as a pair of *real* times $\{t'_j, t_j\}$. These pairs satisfy the system of equations [cf. Eqs. (C8a) and (C19)]:

$$\boldsymbol{K}'_j \cdot \dot{\boldsymbol{K}}'_j = 0, \tag{C21a}$$

$$\frac{\boldsymbol{K}_j^2}{2} = E - \Delta\mathcal{E}_j, \tag{C21b}$$

$$\Delta\mathcal{E}_j = -\frac{\boldsymbol{K}'^2_j + \kappa^2}{2(t_j - t'_j)}\left[\frac{2\dfrac{\boldsymbol{K}_j\cdot\boldsymbol{K}'_j}{t-t'_j} - \boldsymbol{F}'_j\cdot(\boldsymbol{K}_j - \boldsymbol{K}'_j)}{\boldsymbol{F}'^2_j - \boldsymbol{K}'_j\cdot\dot{\boldsymbol{F}}'_j}\right],$$

where $\boldsymbol{K}'_j = \boldsymbol{K}'(t_j,t'_j)$, $\dot{\boldsymbol{K}}'_j = \partial\boldsymbol{K}'(t_j,t'_j)/\partial t'_j$, $\boldsymbol{K}_j = \boldsymbol{K}(t_j,t'_j)$, $\boldsymbol{F}'_j = \boldsymbol{F}(t'_j)$, $\dot{\boldsymbol{F}}'_j = \dot{\boldsymbol{F}}(t'_j)$. Evaluating the integral (12) using the stationary phase method with $\boldsymbol{D}_1(t)$ from (C16) and recalling that $\boldsymbol{D}(t) \approx \boldsymbol{D}_1(t)$ (see Sec. II B), the dipole amplitude $\boldsymbol{D}(\Omega)$ can be presented in the final form (20).

Appendix D: Expansion of the laser-induced dipole near the caustic points

In this Appendix, we seek to show that an expansion of the HHG amplitude in terms of extreme trajectories coincides asymptotically with the results of the present approach. For simplicity, we confine our analysis to the case of a linearly polarized field described by the vector potential $\boldsymbol{A}(t) = \boldsymbol{e}A(t)$, where $\boldsymbol{e}$ is the real polarization vector. For this vector potential, the system of equations (33) can be rewritten in a "scalar" form [see Eqs. (56) and (57) in Ref. [80]]:

$$A(t') - \frac{\int_{t'}^{t} A(\xi)d\xi}{t-t'} = 0, \tag{D1a}$$

$$F(t) + \frac{A(t) - A(t')}{t-t'} = 0. \tag{D1b}$$

where $F(t) = -\partial A(t)/\partial t$. Expanding the left hand sides of the equations in the system (21) near the solutions, $t_j^{(\mathrm{cl})}$ and $t'_j{}^{(\mathrm{cl})}$, of Eq. (D1a), we obtain t'_j and t_j in the form:

$$t'_j{}^{(\pm)} = t'_j{}^{(\mathrm{cl})} \pm \frac{F(t_j{}^{(\mathrm{cl})})}{F(t'_j{}^{(\mathrm{cl})})}\sqrt{\frac{E_{\max}^{(j)} - E}{\zeta_j}}, \tag{D2a}$$

$$t_j^{(\pm)} = t_j{}^{(\mathrm{cl})} \pm \sqrt{\frac{E_{\max}^{(j)} - E}{\zeta_j}}, \tag{D2b}$$

where the $\pm$ signs designate the branches of the square root function and where we have used the notations,

$$\begin{aligned}E_{\max}^{(j)} &= \frac{1}{2}\left[A(t_j{}^{(\mathrm{cl})}) - A(t'_j{}^{(\mathrm{cl})})\right]^2 - \frac{F(t_j{}^{(\mathrm{cl})})}{F(t'_j{}^{(\mathrm{cl})})}I_p, \\ \zeta_j &= -\frac{F^2(t'_j{}^{(\mathrm{cl})})}{2}\left[1 - \frac{F(t_j{}^{(\mathrm{cl})})}{F(t'_j{}^{(\mathrm{cl})})} + \frac{\dot{F}(t_j{}^{(\mathrm{cl})})}{F(t_j{}^{(\mathrm{cl})})}\Delta t_j^{(\mathrm{cl})}\right], \\ &\qquad \Delta t_j^{(\mathrm{cl})} = t_j{}^{(\mathrm{cl})} - t'_j{}^{(\mathrm{cl})}.\end{aligned}$$

Further expanding $\mathcal{S}$ and $\boldsymbol{K}_j\cdot\dot{\boldsymbol{K}}_j$ near the extreme times $t'_j{}^{(\mathrm{cl})}$ and $t_j{}^{(\mathrm{cl})}$, we obtain

$$\begin{aligned}&\mathcal{S}(\boldsymbol{p}_j, t'_j) - \mathcal{S}(\boldsymbol{p}_j, t_j) + \Omega t_j \\ &\approx S(t_j{}^{(\mathrm{cl})}, t'_j{}^{(\mathrm{cl})}) + \Omega t_j{}^{(\mathrm{cl})} \pm \frac{2}{3}\frac{(E_{\max}^{(j)} - E)^{3/2}}{\sqrt{\zeta_j}}, \\ &\boldsymbol{K}_j\cdot\dot{\boldsymbol{K}}_j \approx \mp 2\sqrt{\zeta_j(E_{\max}^{(j)} - E)}.\end{aligned}$$

Substituting these expansions in Eqs. (23), (24), (34), and (35), we obtain $\boldsymbol{d}_j$ in the form:

$$\boldsymbol{d}_j \approx -\theta(E_{\max}^{(j)} - E)\sqrt{i}\frac{C_\kappa}{\pi}\left(\frac{2\kappa^3}{F(t_j'^{(\mathrm{cl})})}\right)^{Z/\kappa} \times \frac{\exp\left[-\frac{\kappa^3}{3F(t_j'^{(\mathrm{cl})})}\right]}{\sqrt{F(t_j'^{(\mathrm{cl})})}} \frac{\exp\left[iS(t_j^{(\mathrm{cl})}, t_j'^{(\mathrm{cl})}) + i\Omega t_j^{(\mathrm{cl})}\right]}{[\Delta t_j^{(\mathrm{cl})}]^{3/2}[\zeta_j(E_{\max}^{(j)} - E)]^{1/4}} \times \sin\left[\frac{2}{3}\frac{(E_{\max}^{(j)} - E)^{3/2}}{\sqrt{\zeta_j}} + \frac{\pi}{4}\right] f_{\mathrm{rec}}(E)\,\boldsymbol{e}. \quad \text{(D3)}$$

The result (D3) can also be obtained by expanding the Airy function in the HHG amplitude of Ref. [80] (see also Ref. [123]) in an asymptotic series for negative arguments. Note that although our analytical calculation is valid for $E < E_{\max}^{(j)}$, the result (D3) can be analytically continued to the region $E > E_{\max}^{(j)}$; the result is that $\sin[\cdots]$ in (D3) should be replaced by the exponent $\exp[-\frac{2}{3}\frac{(E-E_{\max}^{(j)})^{3/2}}{\sqrt{\zeta_j}}]/2$. Thus, the present theory overlaps asymptotically with the results of Ref. [80]. The case of elliptical polarization is more cumbersome to treat analytically and requires a separate analysis.

[1] F. Krausz and M. Ivanov, Attosecond physics, Rev. Mod. Phys. **81**, 163 (2009).

[2] M.-C. Chen, P. Arpin, T. Popmintchev, M. Gerrity, B. Zhang, M. Seaberg, D. Popmintchev, M. M. Murnane, and H. C. Kapteyn, Bright, Coherent, Ultrafast Soft X-Ray Harmonics Spanning the Water Window from a Tabletop Light Source, Phys. Rev. Lett. **105**, 173901 (2010).

[3] T. Popmintchev, M.-C. Chen, D. Popmintchev, P. Arpin, S. Brown, S. Ališauskas, G. Andriukaitis, T. Balčiunas, O. D. Mücke, A. Pugzlys, A. Baltuška, B. Shim, S. E. Schrauth, A. Gaeta, C. Hernández-García, L. Plaja, A. Becker, A. Jaron-Becker, M. M. Murnane, and H. C. Kapteyn, Bright Coherent Ultrahigh Harmonics in the keV X-ray Regime from Mid-Infrared Femtosecond Lasers, Science **336**, 1287 (2012).

[4] D. Popmintchev, B. R. Galloway, M.-C. Chen, F. Dollar, C. A. Mancuso, A. Hankla, L. Miaja-Avila, G. O'Neil, J. M. Shaw, G. Fan, S. Ališauskas, G. Andriukaitis, T. Balčiunas, O. D. Mücke, A. Pugzlys, A. Baltuška, H. C. Kapteyn, T. Popmintchev, and M. M. Murnane, Near- and Extended-Edge X-Ray-Absorption Fine-Structure Spectroscopy Using Ultrafast Coherent High-Order Harmonic Supercontinua, Phys. Rev. Lett. **120**, 093002 (2018).

[5] P. B. Corkum and F. Krausz, Attosecond science, Nat. Phys. **3**, 381 (2007).

[6] L. Plaja, R. Torres, and A. Zaïr, eds., *Attosecond Physics: Attosecond Measurements and Control of Physical Systems* (Springer-Verlag, Berlin, 2013).

[7] T. Schultz and M. Vrakking, eds., *Attosecond and XUV Physics: Ultrafast Dynamics and Spectroscopy* (Wiley-VCH Verlag GmbH & Co., Weinheim, Germany, 2014).

[8] L.-Y. Peng, W.-C. Jiang, J.-W. Geng, W.-H. Xiong, and Q. Gong, Tracing and controlling electronic dynamics in atoms and molecules by attosecond pulses, Phys. Rep. **575**, 1 (2015).

[9] L. DiMauro, M. Frolov, K. L. Ishikawa, and M. Ivanov, 50 years of optical tunneling, J. Phys. B: At. Mol. Opt. Phys. **47**, 200301 (2014).

[10] K. Schafer, Z. Wei, and M. Vrakking, Special issue celebrating 25 years of re-collision physics, J. Phys. B: At. Mol. Opt. Phys. **50**, 170201 (2017).

[11] H. G. Muller, An Efficient Propagation Scheme for the Time-Dependent Schrödinger Equation in the Velocity Gauge, Laser Phys. **9**, 138 (1999).

[12] D. Bauer and P. Koval, QPROP: A Schrödinger-solver for intense laser-atom interaction, Comp. Phys. Comm. **174**, 396 (2006).

[13] V. Mosert and D. Bauer, Photoelectron spectra with QPROP and t-SURFF, Comp. Phys. Comm. **207**, 452 (2016).

[14] V. V. Strelkov, A. A. Gonoskov, I. A. Gonoskov, and M. Yu. Ryabikin, Origin for Ellipticity of High-Order Harmonics Generated in Atomic Gases and the Sublaser-Cycle Evolution of Harmonic Polarization, Phys. Rev. Lett. **107**, 043902 (2011).

[15] V. V. Strelkov, M. A. Khokhlova, A. A. Gonoskov, I. A. Gonoskov, and M. Yu. Ryabikin, High-order harmonic generation by atoms in an elliptically polarized laser field: Harmonic polarization properties and laser threshold ellipticity, Phys. Rev. A **86**, 013404 (2012).

[16] M. V. Frolov, N. L. Manakov, T. S. Sarantseva, A. A. Silaev, N. V. Vvedenskii, and A. F. Starace, Control of threshold enhancements in harmonic generation by atoms in a two-color laser field with orthogonal polarizations, Phys. Rev. A **93**, 023430 (2016).

[17] T. S. Sarantseva, A. A. Silaev, and N. L. Manakov, High-order-harmonic generation in an elliptically polarized laser field: analytic form of the electron wave packet, J. Phys. B: At. Mol. Opt. Phys. **50**, 074002 (2017).

[18] R. Santra and A. Gordon, Three-Step Model for High-Harmonic Generation in Many-Electron Systems, Phys. Rev. Lett. **96**, 073906 (2006).

[19] A. Gordon, F. X. Kärtner, N. Rohringer, and R. Santra, Role of Many-Electron Dynamics in High Harmonic Generation, Phys. Rev. Lett. **96**, 223902 (2006).

[20] S. Sukiasyan, S. Patchkovskii, O. Smirnova, T. Brabec, and M. Yu. Ivanov, Exchange and polarization effect in high-order harmonic imaging of molecular structures, Phys. Rev. A **82**, 043414 (2010).

[21] A. C. Brown, D. J. Robinson, and H. W. van der Hart, Atomic harmonic generation in time-dependent R-matrix theory, Phys. Rev. A **86**, 053420 (2012).

[22] S. Pabst and R. Santra, Strong-Field Many-Body Physics and the Giant Enhancement in the High-Harmonic Spectrum of Xenon, Phys. Rev. Lett. **111**, 233005 (2013).

[23] S. Pabst and R. Santra, Erratum: Strong-Field Many-Body Physics and the Giant Enhancement in the High-Harmonic Spectrum of Xenon [Phys. Rev. Lett. **111**,

233005 (2013)], Phys. Rev. Lett. **112**, 099902 (2014).

[24] D. A. Telnov, K. E. Sosnova, E. Rozenbaum, and S.-I Chu, Exterior complex scaling method in time-dependent density-functional theory: Multiphoton ionization and high-order-harmonic generation of Ar atoms, Phys. Rev. A **87**, 053406 (2013).

[25] O. Hassouneh, A. C. Brown, and H. W. van der Hart, Harmonic generation by noble-gas atoms in the near-IR regime using *ab initio* time-dependent R-matrix theory, Phys. Rev. A **90**, 043418 (2014).

[26] T. Sato, K.L. Ishikawa, I. Březinová, F. Lackner, S. Nagele, and J. Burgdörfer, Time-dependent complete-active-space self-consistent-field method for atoms: Application to high-order harmonic generation, Phys. Rev. A **94**, 023405 (2016).

[27] D. B. Milošević and F. Ehlotzky, Scattering and Reaction Processes in Powerful Laser Fields, Adv. At., Mol., Opt. Phys. **49**, 373 (2003).

[28] A. Becker and F. H. M. Faisal, Intense-field many-body S-matrix theory, J. Phys. B: At. Mol. Opt. Phys. **38**, R1 (2005).

[29] L. V. Keldysh, Ionization in the field of a strong electromagnetic wave, Zh. Eksp. Teor. Fiz. **47**, 1945 (1964) [J. Exp. Theor. Phys. **20**, 1307 (1965)].

[30] A. I. Nikishov and V. I. Ritus, Ionization of systems bound by short-range forces by the field of an electromagnetic wave, Zh. Eksp. Teor. Fiz. **50**, 255 (1966) [J. Exp. Theor. Phys. **23**, 168 (1966)].

[31] A. M. Perelomov, V. S. Popov, and M. V.Terent'ev, Ionization of atoms in an alternating electric field: II, Zh. Eksp. Teor. Fiz. **51**, 309 (1966) [J. Exp. Theor. Phys. **24**, 207 (1967)].

[32] F. H. M. Faisal, Multiple absorption of laser photons by atoms, J. Phys. B: At. Mol. Phys. **6**, L89 (1973).

[33] H. R. Reiss, Effect of an intense electromagnetic field on a weakly bound system, Phys. Rev. A **22**, 1786 (1980).

[34] M. Lewenstein, Ph. Balcou, M. Yu. Ivanov, A. L'Huillier, and P. B. Corkum, Theory of high-harmonic generation by low-frequency laser fields, Phys. Rev. A **49**, 2117 (1994).

[35] M. Yu. Kuchiev and V. N. Ostrovsky, Quantum theory of high-harmonic generation via above-threshold ionization and stimulated recombination, J. Phys. B: At. Mol. Opt. Phys. **32**, L189 (1999).

[36] M. Yu. Kuchiev and V. N. Ostrovsky, Quantum theory of high harmonic generation as a three-step process, Phys. Rev. A **60**, 3111 (1999).

[37] V. V. Strelkov, V. T. Platonenko, A. F. Sterzhantov, and M. Yu. Ryabikin, Attosecond electromagnetic pulses: generation, measurement, and application. Generation of high-order harmonics of an intense laser field for attosecond pulse production, Phys. Usp. **59**, 425 (2016).

[38] D. B. Milošević, Low-frequency approximation for high-order harmonic generation by a bicircular laser field, Phys. Rev. A **97**, 013416 (2018).

[39] P. Salières, B. Carré, L. Le Déroff, F. Grasbon, G. G. Paulus, H. Walther, R. Kopold, W. Becker, D. B. Milošević, A. Sanpera, and M. Lewenstein, Feynman's Path-Integral Approach for Intense-Laser-Atom Interactions, Science **292**, 902 (2001).

[40] D. B. Milošević and W. Becker, Role of long quantum orbits in high-order harmonic generation, Phys. Rev. A **66**, 063417 (2002).

[41] D. B. Milošević, D Bauer, and W. Becker, Quantum-orbit theory of high-order atomic processes in intense laser fields, J. Mod. Opt. **53**, 125 (2006).

[42] O. Smirnova and M. Ivanov, Multielectron high harmonic generation: Simple man on a complex plane, in Ref. [7], p. 201.

[43] L. D. Landau and E. M. Lifshitz, *Quantum Mechanics (Non-relativistic Theory), 3rd Ed.* (Pergamon Press, Oxford, 1977).

[44] A. M. Perelomov and V. S. Popov, Ionization of atoms in an alternating electrical field. III, Zh. Eksp. Teor. Fiz. **52**, 514 (1967) [J. Exp. Theor. Phys. **25**, 336 (1967)].

[45] P. B. Corkum, Plasma Perspective on Strong Field Multiphoton Ionization, Phys. Rev. Lett. **71**, 1994 (1993).

[46] O. Smirnova, M. Spanner, and M. Ivanov, Analytical solutions for strong field-driven atomic and molecular one- and two-electron continua and applications to strong-field problems, Phys. Rev. A **77**, 033407 (2008).

[47] L. Torlina and O. Smirnova, Time-dependent analytical R-matrix approach for strong-field dynamics. I. One-electron systems, Phys. Rev. A **86**, 043408 (2012).

[48] J. Kaushal and O. Smirnova, Nonadiabatic Coulomb effects in strong-field ionization in circularly polarized laser fields, Phys. Rev. A **88**, 013421 (2013).

[49] L. Torlina, F. Morales, J. Kaushal, I. Ivanov, A. Kheifets, A. Zielinski, A. Scrinzi, H. G. Muller, S. Sukiasyan, M. Ivanov, and O. Smirnova, Interpreting attoclock measurements of tunnelling times, Nat. Phys. **11**, 503 (2015).

[50] L. Torlina and O. Smirnova, Coulomb time delays in high harmonic generation, New J. Phys. **19**, 023012 (2017).

[51] M. V. Frolov, N. L. Manakov, A. A. Minina, S. V. Popruzhenko, and A. F. Starace, Adiabatic-limit Coulomb factors for photoelectron and high-order-harmonic spectra, Phys. Rev. A **96**, 023406 (2017).

[52] S. V. Popruzhenko, Coulomb phase in high harmonic generation, J. Phys. B: At. Mol. Opt. Phys. **51**, 144006 (2018).

[53] T. Morishita, A.-T. Le, Z. Chen, and C. D. Lin, Accurate Retrieval of Structural Information from Laser-Induced Photoelectron and High-Order Harmonic Spectra by Few-Cycle Laser Pulses, Phys. Rev. Lett. **100**, 013903 (2008).

[54] M. V. Frolov, N. L. Manakov, T. S. Sarantseva, and A. F. Starace, Analytic confirmation that the factorized formula for harmonic generation involves the exact photorecombination cross section, Phys. Rev. A **83**, 043416 (2011).

[55] O. Smirnova, Y. Mairesse, S. Patchkovskii, N. Dudovich, D. Villeneuve, P. Corkum, and M. Yu. Ivanov, High harmonic interferometry of multi-electron dynamics in molecules, Nature (London) **460**, 972 (2009).

[56] Y. Mairesse, J. Higuet, N. Dudovich, D. Shafir, B. Fabre, E. Mével, E. Constant, S. Patchkovskii, Z. Walters, M. Yu. Ivanov, and O. Smirnova, High Harmonic Spectroscopy of Multichannel Dynamics in Strong-Field Ionization, Phys. Rev. Lett. **104**, 213601 (2010).

[57] D. Shafir, H. Soifer, B. D. Bruner, M. Dagan, Y. Mairesse, S. Patchkovskii, M. Yu. Ivanov, O. Smirnova, and N. Dudovich, Resolving the time when an electron exits a tunnelling barrier,

Nature (London) **485**, 343 (2012).

[58] R. Cireasa, A. E. Boguslavskiy, B. Pons, M. C. H. Wong, D. Descamps, S. Petit, H. Ruf, N. Thiré, A. Ferré, J. Suarez, J. Higuet, B. E. Schmidt, A. F. Alharbi, F. Légaré, V. Blanchet, B. Fabre, S. Patchkovskii, O. Smirnova, Y. Mairesse, and V. R. Bhardwaj, Probing molecular chirality on a sub-femtosecond timescale, Nat. Phys. **11**, 654 (2015).

[59] O. Pedatzur, G. Orenstein, V. Serbinenko, H. Soifer, B. D. Bruner, A. J. Uzan, D. S. Brambila, A. G. Harvey, L. Torlina, F. Morales, O. Smirnova, and N. Dudovich, Attosecond tunnelling interferometry, Nat. Phys. **11**, 815 (2015).

[60] B. D. Bruner, Z. Mašín, M. Negro, F. Morales, D. Brambila, M. Devetta, D. Faccialà, A. G. Harvey, M. Ivanov, Y. Mairesse, S. Patchkovskii, V. Serbinenko, H. Soifer, S. Stagira, C. Vozzi, N. Dudovich, and O. Smirnova, Multidimensional high harmonic spectroscopy of polyatomic molecules: detecting sub-cycle laser-driven hole dynamics upon ionization in strong mid-IR laser fields, Faraday Discuss. **194**, 369–405 (2016).

[61] O. Smirnova, Y. Mairesse, and S. Patchkovskii, Opportunities for chiral discrimination using high harmonic generation in tailored laser fields, J. Phys. B: At. Mol. Opt. Phys. **48**, 234005 (2015).

[62] D. Ayuso, P. Decleva, S. Patchkovskii, and O. Smirnova, Chiral dichroism in bi-elliptical high-order harmonic generation, J. Phys. B: At. Mol. Opt. Phys. **51**, 06LT01 (2018).

[63] D. Ayuso, P. Decleva, S. Patchkovskii, and O. Smirnova, Strong-field control and enhancement of chiral response in bi-elliptical high-order harmonic generation: an analytical model, J. Phys. B: At. Mol. Opt. Phys. **51**, 124002 (2018).

[64] Á. Jiménez-Galán, N. Zhavoronkov, M. Schloz, F. Morales, and M. Ivanov, Time-resolved high harmonic spectroscopy of dynamical symmetry breaking in bi-circular laser fields: the role of Rydberg states, Opt. Express **25**, 22880 (2017).

[65] Á. Jiménez-Galán, N. Zhavoronkov, D. Ayuso, F. Morales, S. Patchkovskii, M. Schloz, E. Pisanty, O. Smirnova, and M. Ivanov, Control of attosecond light polarization in two-color bicircular fields, Phys. Rev. A **97**, 023409 (2018).

[66] D. Ayuso, A. Jiménez-Galán, F. Morales, M. Ivanov, and O. Smirnova, Attosecond control of spin polarization in electron–ion recollision driven by intense tailored fields, New J. Phys. **19**, 073007 (2017).

[67] Yu. N. Demkov and V. N. Ostrovsky, *Zero-Range Potentials and Their Applications in Atomic Physics* (Plenum, New York, 1988).

[68] N. L. Manakov and L. P. Rapoport, Particle with low binding energy in a circularly polarized field, Zh. Eksp. Teor. Fiz. **69**, 842 (1975) [J. Exp. Theor. Phys. **42**, 430 (1976)].

[69] I. J. Berson, Multiphoton ionization and stimulated bremsstrahlung radiation in the case of short-range potentials, J. Phys. B: At. Mol. Phys. **8**, 3078 (1975).

[70] N. L. Manakov and A. G. Fainshtein, Decay of a weakly bound level in a monochromatic field, Zh. Eksp. Teor. Fiz. **79**, 751 (1980) [J. Exp. Theor. Phys. **52**, 382 (1980)].

[71] W. Becker, S. Long, and J. K. McIver, Higher-harmonic production in a model atom with short-range potential, Phys. Rev. A **41**, 4112 (1990).

[72] W. Becker, S. Long, and J. K. McIver, Modeling harmonic generation by a zero-range potential, Phys. Rev. A **50**, 1540 (1994).

[73] M. V. Frolov, N. L. Manakov, E. A. Pronin, and A. F. Starace, Model-Independent Quantum Approach for Intense Laser Detachment of a Weakly Bound Electron, Phys. Rev. Lett. **91**, 053003 (2003).

[74] M. V. Frolov, N. L. Manakov, and A. F. Starace, Effective-range theory for an electron in a short-range potential and a laser field, Phys. Rev. A **78**, 063418 (2008).

[75] S. P. Andreev, B. M. Karnakov, V. D. Mur, and V. A. Polunin, Spectrum of weakly bound states of a particle in external electric fields, Zh. Eksp. Teor. Fiz. **86**, 866 (1984) [J. Exp. Theor. Phys. **59**, 506 (1984)].

[76] S. P. Andreev, B. M. Karnakov, and V. D. Mur, Energy spectrum of a particle in potentials with strongly differing ranges, Theor. Math. Phys. **64**, 838 (1985).

[77] N. L. Manakov, V. D. Ovsiannikov, and L. P. Rapoport, Atoms in a laser field, Phys. Rep. **141**, 320 (1986).

[78] M. V. Frolov, A. V. Flegel, N. L. Manakov, and A. F. Starace, Description of harmonic generation in terms of the complex quasienergy. I. General formulation, Phys. Rev. A **75**, 063407 (2007).

[79] M. V. Frolov, N. L. Manakov, A. A. Silaev, N. V. Vvedenskii, and A. F. Starace, High-order harmonic generation by atoms in a few-cycle laser pulse: Carrier-envelope phase and many-electron effects, Phys. Rev. A **83**, 021405 (R) (2011).

[80] M. V. Frolov, N. L. Manakov, A. M. Popov, O. V. Tikhonova, E. A. Volkova, A. A. Silaev, N. V. Vvedenskii, and A. F. Starace, Analytic theory of high-order-harmonic generation by an intense few-cycle laser pulse, Phys. Rev. A **85**, 033416 (2012).

[81] Y. Okajima, O. I. Tolstikhin, and T. Morishita, Adiabatic theory of high-order harmonic generation: One-dimensional zero-range-potential model, Phys. Rev. A **85**, 063406 (2012).

[82] M. V. Frolov, N. L. Manakov, T. S. Sarantseva, and A. F. Starace, Analytic formulae for high harmonic generation, J. Phys. B: At. Mol. Opt. Phys. **42**, 035601 (2009).

[83] M. V. Frolov, N. L. Manakov, T. S. Sarantseva, M. Yu. Emelin, M. Yu. Ryabikin, and A. F. Starace, Analytic Description of the High-Energy Plateau in Harmonic Generation by Atoms: Can the Harmonic Power Increase with Increasing Laser Wavelengths? Phys. Rev. Lett. **102**, 243901 (2009).

[84] M. V. Frolov, N. L. Manakov, T. S. Sarantseva, and A. F. Starace, High-order-harmonic-generation spectroscopy with an elliptically polarized laser field, Phys. Rev. A **86**, 063406 (2012).

[85] T. S. Sarantseva, M. V. Frolov, N. L. Manakov, M. Yu. Ivanov, and A. F. Starace, Harmonic generation spectroscopy with a two-colour laser field having orthogonal linear polarizations, J. Phys. B: At. Mol. Opt. Phys. **46**, 231001 (2013).

[86] S. Minemoto, T. Umegaki, Y. Oguchi, T. Morishita, A.-T. Le, S. Watanabe, and H. Sakai, Retrieving photorecombination cross sections of atoms from high-order

harmonic spectra, Phys. Rev. A **78**, 061402 (R) (2008).

[87] A.-T. Le, T. Morishita, and C. D. Lin, Extraction of the species-dependent dipole amplitude and phase from high-order harmonic spectra in rare-gas atoms, Phys. Rev. A **78**, 023814 (2008).

[88] D. D. Hickstein, F. J. Dollar, P. Grychtol, J. L. Ellis, R. Knut, C. Hernández-García, D. Zusin, C. Gentry, J. M. Shaw, T. Fan, K. M. Dorney, A. Becker, A. Jaroń-Becker, H. C. Kapteyn, M. M. Murnane, and C. G. Durfee, Non-collinear generation of angularly isolated circularly polarized high harmonics, Nat. Photon. **9**, 743 (2015).

[89] P.-C. Huang, C. Hernández-García, J.-T. Huang, P.-Y. Huang, C.-H. Lu, L. Rego, D. D. Hickstein, J. L. Ellis, A. Jaron-Becker, A. Becker, S.-D. Yang, C. G. Durfee, L. Plaja, H. C. Kapteyn, M. M. Murnane, A. H. Kung, and M.-C. Chen, Polarization control of isolated high-harmonic pulses, Nat. Photon. **12**, 349 (2018).

[90] O. I. Tolstikhin, T. Morishita, and S. Watanabe, Adiabatic theory of ionization of atoms by intense laser pulses: One-dimensional zero-range-potential model, Phys. Rev. A **81**, 033415 (2010).

[91] O. I. Tolstikhin and T. Morishita, Adiabatic theory of ionization by intense laser pulses: Finite-range potentials, Phys. Rev. A **86**, 043417 (2012).

[92] P. L. Kapitza, Dynamical stability of a pendulum when its point of suspension vibrates, Zh. Eksp. Teor. Fiz. **21**, 588 (1951) [in Russian].

[93] L. D. Landau and E. M. Lifshitz, *Mechanics, 3rd Ed.* (Elsevier, Oxford, 1976).

[94] H. Eichmann, A. Egbert, S. Nolte, C. Momma, B. Wellegehausen, W. Becker, S. Long, and J. K. McIver, Polarization-dependent high-order two-color mixing, Phys. Rev. A **51**, R3414 (1995).

[95] D. B. Milošević, W. Becker, and R. Kopold, Generation of circularly polarized high-order harmonics by two-color coplanar field mixing, Phys. Rev. A **61**, 063403 (2000).

[96] A. Ferré, C. Handschin, M. Dumergue, F. Burgy, A. Comby, D. Descamps, B. Fabre, G. A. Garcia, R. Géneaux, L. Merceron, E. Mével, L. Nahon, S. Petit, B. Pons, D. Staedter, S. Weber, T. Ruchon, V. Blanchet, and Y. Mairesse, A table-top ultrashort light source in the extreme ultraviolet for circular dichroism experiments, Nat. Photon. **9**, 93 (2015).

[97] O. Kfir, P. Grychtol, E. Turgut, R. Knut, D. Zusin, D. Popmintchev, T. Popmintchev, H. Nembach, J. M. Shaw, A. Fleischer, H. Kapteyn, M. Murnane, and O. Cohen, Generation of bright phase-matched circularly-polarized extreme ultraviolet high harmonics, Nat. Photon. **9**, 99 (2015).

[98] D. B. Milošević, Generation of elliptically polarized attosecond pulse trains, Opt. Lett. **40**, 2381 (2015).

[99] L. Medišauskas, J. Wragg, H. van der Hart, and M. Yu. Ivanov, Generating Isolated Elliptically Polarized Attosecond Pulses Using Bichromatic Counterrotating Circularly Polarized Laser Fields, Phys. Rev. Lett. **115**, 153001 (2015).

[100] T. Fan, P. Grychtol, R. Knut, C. Hernández-García, D. D. Hickstein, D. Zusin, C. Gentry, F. J. Dollar, C. A. Mancuso, C. W. Hogle, O. Kfir, D. Legut, K. Carva, J. L. Ellis, K. M. Dorney, C. Chen, O. G. Shpyrko, E. E. Fullerton, O. Cohen, P. M. Oppeneer, D. B. Milošević, A. Becker, A. A. Jaroń-Becker, T. Popmintchev, M. M. Murnane, and H. C. Kapteyn, Bright circularly polarized soft X-ray high harmonics for X-ray magnetic circular dichroism, Proc. Nat. Acad. Sci. USA **112**, 14206 (2015).

[101] D. Baykusheva, M. S. Ahsan, N. Lin, and H. J. Wörner, Bicircular High-Harmonic Spectroscopy Reveals Dynamical Symmetries of Atoms and Molecules, Phys. Rev. Lett. **116**, 123001 (2016).

[102] C. Hernández-García, C. G. Durfee, D. D. Hickstein, T. Popmintchev, A. Meier, M. M. Murnane, H. C. Kapteyn, I. J. Sola, A. Jaron-Becker, and A. Becker, Schemes for generation of isolated attosecond pulses of pure circular polarization, Phys. Rev. A **93**, 043855 (2016).

[103] O. Kfir, P. Grychtol, E. Turgut, R. Knut, D. Zusin, A. Fleischer, E. Bordo, T. Fan, D. Popmintchev, T. Popmintchev, H. Kapteyn, M. Murnane, and O. Cohen, Helicity-selective phase-matching and quasi-phase matching of circularly polarized high-order harmonics: towards chiral attosecond pulses, J. Phys. B: At. Mol. Opt. Phys. **49**, 123501 (2016).

[104] M. Ivanov and E. Pisanty, High-harmonic generation: Taking control of polarization, Nat. Photon. **8**, 501 (2014).

[105] A. Fleischer, O. Kfir, T. Diskin, P. Sidorenko, and O. Cohen, Spin angular momentum and tunable polarization in high-harmonic generation, Nat. Photon. **8**, 543 (2014).

[106] E. Pisanty, S. Sukiasyan, and M. Ivanov, Spin conservation in high-order-harmonic generation using bicircular fields, Phys. Rev. A **90**, 043829 (2014).

[107] D. B. Milošević, High-order harmonic generation by a bichromatic elliptically polarized field: conservation of angular momentum, J. Phys. B: At. Mol. Opt. Phys. **48**, 171001 (2015).

[108] S. Odžak, E. Hasović, and D. B. Milošević, High-order harmonic generation in polyatomic molecules induced by a bicircular laser field, Phys. Rev. A **94**, 033419 (2016).

[109] M. V. Frolov, N. L. Manakov, A. A. Minina, N. V. Vvedenskii, A. A. Silaev, M. Yu. Ivanov, and A. F. Starace, Control of Harmonic Generation by the Time Delay Between Two-Color, Bicircular Few-Cycle Mid-IR Laser Pulses, Phys. Rev. Lett. **120**, 263203 (2018).

[110] D. B. Milošević, Control of the helicity of high-order harmonics generated by bicircular laser fields, Phys. Rev. A **98**, 033405 (2018).

[111] C. D. Stanciu, F. Hansteen, A. V. Kimel, A. Kirilyuk, A. Tsukamoto, A. Itoh, and Th. Rasing, All-Optical Magnetic Recording with Circularly Polarized Light, Phys. Rev. Lett. **99**, 047601 (2007).

[112] J.-Y. Bigot, M. Vomir, and E. Beaurepaire, Coherent ultrafast magnetism induced by femtosecond laser pulses, Nat. Phys. **5**, 515 (2009).

[113] O. Kfir, S. Zayko, C. Nolte, M. Sivis, M. Möller, B. Hebler, S. S. P. K. Arekapudi, D. Steil, S. Schäfer, M. Albrecht, O. Cohen, S. Mathias, and C. Ropers, Nanoscale magnetic imaging using circularly polarized high-harmonic radiation, Sci. Adv. **3**, eaao4641 (2017).

[114] A. D. Bandrauk, F. Mauger, and K.-J. Yuan, Circularly polarized harmonic generation by intense bicircular laser pulses: electron recollision dynamics and frequency dependent helicity, J. Phys. B: At. Mol. Opt. Phys. **49**, 23LT01 (2016).

[115] D. B. Milošević, Circularly polarized high harmonics generated by a bicircular field from inert atomic gases in the p state: A tool for exploring chirality-sensitive processes, Phys. Rev. A **92**, 043827 (2015).

[116] N. L. Manakov, M. V. Frolov, A. F. Starace, and I. I. Fabrikant, Interaction of laser radiation with a negative ion in the presence of a strong static electric field, J. Phys. B: At. Mol. Opt. Phys. **33**, R141 (2000).

[117] M. V. Frolov, D. V. Knyazeva, N. L. Manakov, J.-W. Geng, L.-Y. Peng, and A. F. Starace, Analytic model for the description of above-threshold ionization by an intense short laser pulse, Phys. Rev. A **89**, 063419 (2014).

[118] S. P. Goreslavskii and S. V. Popruzhenko, Differential photoelectron distributions in a strong elliptically polarized low-frequency laser field, Zh. Eksp. Teor. Fiz. **110**, 1200 (1996) [J. Exp. Theor. Phys. **83**, 661 (1996)].

[119] A. A. Minina, M. V. Frolov, A. N. Zheltukhin, and N. V. Vvedenskii, Tunnelling approximation for estimating the amplitude of high harmonic generation in intense laser fields: analysis of ionisation and recombination times, Quantum Electron. **47**, 216 (2017).

[120] O. Raz, O. Pedatzur, B. D. Bruner, and N. Dudovich, Spectral caustics in attosecond science, Nat. Photon. **6**, 170 (2012).

[121] D. Faccialà, S. Pabst, B. D. Bruner, A. G. Ciriolo, S. De Silvestri, M. Devetta, M. Negro, H. Soifer, S. Stagira, N. Dudovich, and C. Vozzi, Probe of Multielectron Dynamics in Xenon by Caustics in High-Order Harmonic Generation, Phys. Rev. Lett. **117**, 093902 (2016).

[122] D. Faccialà, S. Pabst, B. D. Bruner, A. G. Ciriolo, M. Devetta, M. Negro, P. P. Geetha, A. Pusala, H. Soifer, N. Dudovich, S. Stagira, and C. Vozzi, High-order harmonic generation spectroscopy by recolliding electron caustics, J. Phys. B: At. Mol. Opt. Phys. **51**, 134002 (2018).

[123] M. V. Frolov, N. L. Manakov, W.-H. Xiong, L.-Y. Peng, J. Burgdörfer, and A. F. Starace, Scaling laws for high-order-harmonic generation with midinfrared laser pulses, Phys. Rev. A **92**, 023409 (2015).

[124] S. V. Popruzhenko and D. Bauer, Strong field approximation for systems with Coulomb interaction, J. Mod. Opt. **55**, 2573 (2008).

[125] S. V. Popruzhenko, Keldysh theory of strong field ionization: history, applications, difficulties and perspectives, J. Phys. B: At. Mol. Opt. Phys. **47**, 204001 (2014).

[126] S. V. Popruzhenko, Invariant Form of Coulomb Corrections in the Theory of Nonlinear Ionization of Atoms by Intense Laser Radiation, Zh. Eksp. Teor. Fiz. **145**, 664 (2014) [J. Exp. Theor. Phys. **118**, 580 (2014)].

[127] X. M. Tong and C. D. Lin, Empirical formula for static field ionization rates of atoms and molecules by lasers in the barrier-suppression regime, J. Phys. B: At. Mol. Opt. Phys. **38**, 2593 (2005).

[128] O. E. Alon, V. Averbukh, and N. Moiseyev, Selection Rules for the High Harmonic Generation Spectra, Phys. Rev. Lett. **80**, 3743 (1998).

[129] L. D. Landau and E. M. Lifshitz, *The Classical Theory of Fields, 4th Ed.* (Pergamon Press, Oxford, 1975).

[130] K. Blum, *Density Matrix Theory and Applications, 3rd Ed.* (Springer-Verlag, Berlin, 2012).

[131] A. A. Silaev, A. A. Romanov, and N. V. Vvedenskii, Multi-hump potentials for efficient wave absorption in the numerical solution of the time-dependent Schrödinger equation, J. Phys. B: At. Mol. Opt. Phys. **51**, 065005 (2018).

[132] A. V. Flegel, M. V. Frolov, N. L. Manakov, and A. F. Starace, Circularly polarized laser field-induced rescattering plateaus in electron-atom scattering, Phys. Lett. A **334**, 197 (2005).

[133] K. Huang and C. N. Yang, Quantum-Mechanical Many-Body Problem with Hard-Sphere Interaction, Phys. Rev. **105**, 767 (1957).

[134] A. Derevianko, Revised Huang-Yang multipolar pseudopotential, Phys. Rev. A **72**, 044701 (2005).